

Specific heat and magnetic susceptibility of the spinels GeNi_2O_4 and GeCo_2O_4

J. C. Lashley,¹ R. Stevens,² M. K. Crawford,³ J. Boerio-Goates,² B. F. Woodfield,² Y. Qiu,^{4,5} J. W. Lynn,⁴ P. A. Goddard,^{1,6} and R. A. Fisher¹

¹*Los Alamos National Laboratory, Los Alamos, New Mexico 87545, USA*

²*Department of Chemistry and Biochemistry, Brigham Young University, Provo, Utah 84602, USA*

³*Central Research and Development Department, DuPont, E400/5424, Wilmington, Delaware 19880, USA*

⁴*NIST Center for Neutron Research, Gaithersburg, Maryland 20899, USA*

⁵*Department of Materials Science and Engineering, University of Maryland, College Park, Maryland 20742, USA*

⁶*Clarendon Laboratory, University of Oxford, Parks Road, Oxford OX1 3PU, United Kingdom*

(Received 29 January 2008; revised manuscript received 29 April 2008; published 11 September 2008)

Specific-heat and magnetic-susceptibility measurements are reported for the polycrystalline spinel compounds GeNi_2O_4 and GeCo_2O_4 in magnetic fields up to 14 T and $0.5 \text{ K} \leq T \leq 400 \text{ K}$. Both compounds have first-order antiferromagnetic transitions. There are two sharp closely spaced magnetic-ordering anomalies for GeNi_2O_4 at Néel temperatures $T_{N1}(0) = 12.080 \text{ K}$ and $T_{N2}(0) = 11.433 \text{ K}$ in zero magnetic field. There is also a broad anomaly in the specific heat centered at $\sim 5 \text{ K}$, which is present for all fields. Spin waves with an average gap of 10.9 K are associated with this anomaly, which is confirmed by neutron-scattering measurements. An unusual feature of the antiferromagnetism for GeNi_2O_4 is the simultaneous presence of both gapped and ungapped spin waves in the Néel state, inferred from the specific-heat data. GeCo_2O_4 has a single anomaly at $T_N(0) = 20.617 \text{ K}$ in zero magnetic field. Spin waves with an average gap of 38.7 K are derived from fitting the low-temperature specific heat and are also observed by neutron scattering. For both compounds $\sim 50\%$ of the derived magnetic entropy is below the ordering temperatures, and the total magnetic entropies are only $\sim 60\%$ of that predicted for the Ni^{2+} and Co^{2+} single-ion ground-state configurations. The missing entropy is not linked to magnetic disorder in the ground state or hidden ordering below 0.5 K. It is postulated that the missing entropy is accounted for by the presence of substantial magnetic correlations well above the Néel temperatures. Fitting the GeNi_2O_4 susceptibilities to the Curie-Weiss law yields parameters that are consistent with those found for Ni^{2+} ions in a crystal-electric-field environment including octahedral and trigonal components. The application of the Curie-Weiss law to the GeCo_2O_4 susceptibilities is not valid because of low-lying crystal-electric-field states.

DOI: [10.1103/PhysRevB.78.104406](https://doi.org/10.1103/PhysRevB.78.104406)

PACS number(s): 65.40.Ba, 75.40.Cx, 75.30.Ds

I. INTRODUCTION

Normal spinels have a face-centered-cubic (fcc) crystal structure with composition AB_2O_4 , where A and B are metal ions. The A ions occupy tetrahedral sites and the B ions are on octahedral (cubic) sites located on the corners of vertex-sharing tetrahedra. Of particular interest is the case where the B ions are magnetic and order antiferromagnetically (AF), which may lead to frustration. There are four principal magnetic axes oriented at 109° to one another that are crystallographically equivalent. Figure 1 shows the magnetic structure of the spinels for the B ions. The magnetic order in both GeNi_2O_4 (GNO) and GeCo_2O_4 (GCO) is characterized by ferromagnetic (111) planes and a $[\frac{1}{2}, \frac{1}{2}, \frac{1}{2}]$ magnetic propagation vector.¹ This can lead to the formation of four magnetic domains due to the four equivalent $\langle 111 \rangle$ directions, ignoring the possibility that the spins might align in different symmetry related directions with respect to the (111) planes. Furthermore, a distortion of the crystal from cubic symmetry to tetragonal symmetry in GCO can choose one of three possible directions as the unique axis, leading to three structural domains. Therefore, it is possible for a compound such as GCO to have as many as 12 different magnetic domains. In a magnetic field (B) of sufficient strength, the number of domains can be reduced. To apply a magnetic field parallel or perpendicular to an ordering axis in a single crystal, it is

necessary to have a single magnetic domain, which would probably form only below the Néel temperature (T_N) for a sufficiently large B . However, in the paramagnetic phase, because of the four equivalent tetrahedral axes, it is not possible to measure the anisotropy in physical properties such as the specific heat or magnetic susceptibility.

A Ni^{2+} ion ($3d^8$; 3F_4 ; $L=3$, $S=1$) in an octahedral crystal field will have an orbital-singlet ground state with $S=1$. In GNO there is also a weaker trigonal crystal electric field at the Ni^{2+} sites which have D_{3d} symmetry. This trigonal crystal field and the presence of second-order spin-orbit-induced coupling between the higher crystal-field states and the spin-triplet ground state will cause additional splitting of the ground state into two levels, a doublet and a singlet. The non-Kramers doublet is usually the ground state and additional interactions can split this doublet as well. The splitting within the $S=1$ manifold is usually much smaller in energy ($< 1 \text{ K}$) than that associated with the magnetic ordering.² Antiferromagnetic ordering of these moments will lead to spin-wave excitations, which will have either a gapped or ungapped (T^3 temperature dependence) contribution to the low-temperature specific heat (C). The next higher Ni^{2+} crystal-field (CF) state is $\sim 12\,400 \text{ K}$ above the ground state and has no measurable Schottky contribution to the specific heat below 400 K. For sufficiently high temperatures, the expected entropy related to the antiferromagnetic ordering is $2R \ln(2S+1) = 2R \ln 3$ per mole of GNO.

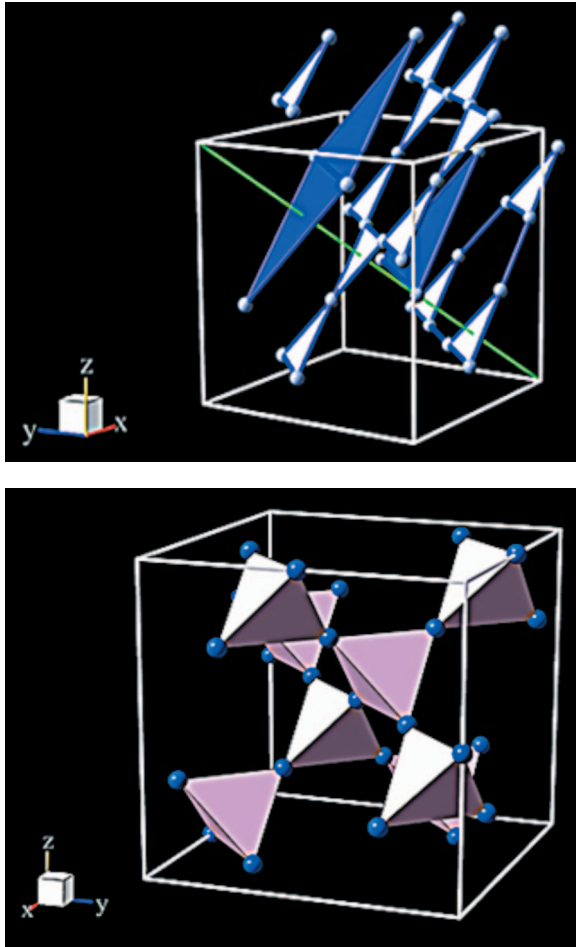


FIG. 1. (Color) The two figures are different illustrations of the spinel structure, AB_2O_4 , with the magnetic ions (Ni^{2+} or Co^{2+} in this paper) represented by the light- or dark-blue spheres on the B sites. (The crystallographic structure is face-centered cubic and the Ge and O ions on the A site are omitted for clarity.) Top panel: White triangles represent the kagome (111) planes—a kagome lattice is a repeat pattern of a hexagon plus six equilateral triangles attached to the hexagon sides—and the dark-blue triangles represent the (111) triangular planes. The green diagonal line is one of four equivalent $\langle 111 \rangle$ axes connecting opposite corners of the unit cell. There is a trigonal crystal electric field at the magnetic ions. The magnetic ions in the two planes (kagome and triangular) are ordered ferromagnetically, while the ordering between plane-to-plane sets is antiferromagnetic (Ref. 1). Bottom figure: This figure shows connected tetrahedra with the magnetic ions located on the corners. Three magnetic ions at the corners of the tetrahedra bases form the kagome planes and those on the vertices are in the triangular planes. The ratio of the number of magnetic ions in kagome planes versus those in triangular planes is $3/1$.

A Co^{2+} ion ($3d^7$; ${}^4F_{9/2}$; $L=3$, $S=3/2$) in an octahedral crystal field has the $L=3$ manifold split into a series of well-separated states. The ground-state orbital angular momentum can be taken as a “fictitious” $L=1$, which couples to the spin, $S=3/2$, through spin-orbit coupling ($\lambda L \cdot S$) to form three separated sets of energy manifolds, i.e., $J=1/2$, $3/2$, and $5/2$, with the ground state usually $J=1/2$.³ Above T_N , GCO also has a trigonal crystal-electric-field component at the Co^{2+}

sites; at T_N there is, in addition, a cubic-to-tetragonal transition, which will introduce a weak tetragonal crystal field as well. The trigonal field splits the $J=1/2$, $3/2$, and $5/2$ manifolds into six Kramers doublets at 0, 180, 360, 440, 1760, and 1930 K, with additional splitting and removal of all degeneracy in magnetic fields. These levels were determined using inelastic neutron scattering.⁴ There are Schottky-type contributions to the specific heat in the temperature range of interest [$0 \text{ K} \leq T \leq 75 \text{ K}$] from some of these crystal-field levels, which must be taken into account in the analysis of the specific-heat data—see Sec. IV B. At sufficiently high temperatures, after correction for the specific-heat contribution from the crystal-field states, the expected entropy associated with the antiferromagnetic ordering is $2R \ln(2J+1) = 2R \ln 2$ per mole of GCO. Below T_N there will be antiferromagnetic spin-wave excitations in the $J=1/2$ levels.

The magnetic spinels GNO and GCO were selected for the present investigations because Ni^{2+} has an essentially spin-only ground state, $S=1$, while Co^{2+} has an anisotropic Kramers doublet ground-state, $J=1/2$, with unquenched orbital angular momentum. One goal of the research was to ascertain if magnetic ordering in the spinels is influenced by different ground states, i.e., one with spin-only coupling and the other with spin-orbit coupling. Both compounds order antiferromagnetically: GNO has two sharp closely spaced first-order transitions at $T_{N1}(0)=12.080 \text{ K}$ and $T_{N2}(0)=11.433 \text{ K}$. There is a very much smaller anomaly centered at $\sim 11 \text{ K}$ for $B=0$ and 1 T of unknown origin and a fourth broadened anomaly centered at $\sim 5 \text{ K}$ for all fields that is probably associated with an exchange enhanced splitting of the $S=1$ ground state. GCO has a single sharp first-order transition at $T_N(0)=20.617 \text{ K}$, which is accompanied by a field-dependent crystallographic transition from cubic-to-tetragonal symmetry.^{4,5}

A previously published paper⁵ reported results of measurements made on the same polycrystalline GNO sample used for the present experiments: specific heats in zero magnetic field, magnetic susceptibilities (χ), synchrotron x-ray powder diffraction, and neutron powder diffraction. In preparation is a similar paper reporting results for the same types of measurements for GCO.⁴ In those papers the zero-field specific heat is analyzed to determine the lattice contribution (C_{lat}), the magnetic specific heat (C_{mag}) and entropy (S_{mag}), and spin-wave parameters characterizing the antiferromagnetic ordering. However only a very brief outline of the specific-heat and magnetic-susceptibility data analysis and results is given. Although the magnetic entropies recovered at 75 K for both compounds are significantly less than the expected $2R \ln(2S+1)$ or $2R \ln(2J+1)$, neither compound is fully magnetically frustrated nor has “hidden” ordering below the lowest measurement temperatures. The missing entropy is attributed to magnetic correlations well above 75 K. This paper significantly extends the scope of those measurements:^{4,5} It reports results for specific-heat measurements in magnetic fields up to 14 T and magnetic susceptibilities up to 7 T, and it provides a detailed and comprehensive description of the data-analysis procedures used to extract microscopic parameters. The specific heats in magnetic fields prove that neither compound exhibits evidence of ground-state degeneracy nor is it probable that the missing

entropy is a consequence of hidden ordering below the lowest temperatures of the measurements. The results of the in-field measurements are also used to demonstrate how the spin waves characterizing the antiferromagnetic order evolve with magnetic field. Another paper,⁶ also in preparation, reports measurements of the magnetocaloric effect, specific heats, and magnetization in pulsed and fixed magnetic fields up to 45 T for the same two samples. It extends but does not duplicate the results reported in this paper.

Section II presents details of the experimental procedures including sample preparation. Section III reports the experimental results for the specific-heat and the susceptibility measurements and their analysis. Section IV outlines the methods used for the specific-heat data analysis, the analyses, and a discussion of the results. Section V summarizes previously published specific-heat and magnetization/susceptibility measurements made by other research groups. Section VI contains a summary and conclusions.

II. EXPERIMENT

Polycrystalline GNO and GCO were synthesized at DuPont using standard solid-state techniques. Stoichiometric mixtures of GeO_2 and either NiO or CoO were reacted by firing in air at 1473 K. A detailed description of the preparations and characterizations is given in Ref. 7, which also tabulates the experimental specific-heat data and the standard thermodynamic functions for $B=0$.

The specific heat for $B=0$ was measured for both GNO and GCO at Brigham Young University (BYU) in the range $0.5 \text{ K} \leq T \leq 400 \text{ K}$ using semiadiabatic, isothermal, and adiabatic heat-pulse methods.^{8,9} Those measurements have an estimated accuracy of $\sim 0.5\%$ with a precision of $\sim 0.1\%$. Specific heats up to 14 T were measured at the Los Alamos National Laboratory (LANL) by a relaxation technique using a Quantum Design Physical Properties Measurement System (PPMS).¹⁰ Two PPMS cryostats were used for the measurements: One had a maximum field of 9 T and the other 14 T. There are small differences in thermometer calibrations for the two cryostats. Measurements were made with the second PPMS for $B=0, 9, 9.5, 10, 10.5, 11, 12,$ and 14 T. A comparison of the specific heats at $B=0$ and 9 T showed a small offset in the data for the two devices, probably due to differences in their temperature scales. The two data sets were used to correct the temperatures for the second PPMS, which put the specific-heat measurements for the two cryostats into register for $B=0$ and 9 T. An average accuracy and precision for a PPMS specific-heat apparatus, properly used, is $\sim 2\%$, but it can become larger at low temperatures depending on sample size.¹⁰ While the combined in-field measurements are adequate to show overall qualitative magnetic-field effects, only those measurements made with the first PPMS up to 9 T were used in analysis of in-field specific-heat data. For GNO the applied fields were 0, 1, 3, 5, 7, 9, 9.5, 10, 11, 12, 13, and 14 T in the temperature range $1.8 \text{ K} \leq T \leq 30 \text{ K}$; and for GCO the fields were 0, 1, 3, 5, 7, 9, 9.5, 10, 10.5, 11, 12, and 14 T in the range $1.8 \text{ K} \leq T \leq 65 \text{ K}$. The same samples were used for both the BYU and LANL specific-heat measurements. For $B=0$ the $\pm 2\% - \pm 3\%$ agreement between the

two data sets is satisfactory and within their combined accuracies. All specific-heat analyses for measurements in $B=0$ use the more accurate BYU data.

The magnetization/susceptibility measurements were made at DuPont using a Quantum Design MPMS-XL superconducting quantum interference device (SQUID) magnetometer. The accuracy is $\sim 1\%$ with a precision of $\sim 0.1\%$. For both samples measurements were made in magnetic fields of 0.001, 0.01, 0.1, 1, 2, 5, and 7 T for $2 \text{ K} \leq T \leq 400 \text{ K}$.

Neutron-scattering measurements were made using the NG4 disk chopper time-of-flight spectrometer (DCS) at the NIST Center for Neutron Research.¹¹ The DCS uses choppers to create pulses of monochromatic neutrons whose energy transfers on scattering are determined by their arrival times in the instrument's 913 detectors located at scattering angles from -30° to 140° . The measurements were performed using neutrons with incident wavelengths between 3.0 and 5.0 Å, with corresponding elastic-energy resolution widths between 0.45 and 0.11 meV full widths at half maximums.

All temperature measurements were made on thermometers with calibrations traceable to the ITS-90 temperature scale.

III. RESULTS

This section presents experimental results for specific-heat and magnetic-susceptibility measurements on polycrystalline GNO and GCO in magnetic fields up to 14 T. The specific-heat results are in Sec. III A. A discussion of the susceptibility measurements and derived parameters characterizing them is in Sec. III B.

A. Specific heats

1. Specific heats of GeNi_2O_4 and GeCo_2O_4 in zero magnetic field

Figures 2 and 3 are plots of the total specific heat for $B=0$: C/T vs T for GNO and GCO, respectively. These data were measured⁷ at BYU and are analyzed to obtain the field-independent C_{lat} to 75 K, the magnetic entropy, and parameters characterizing the antiferromagnetic ordering.^{4,5} The ordering anomalies are very narrow, as shown on an expanded scale in the insets of the figures, and their shapes suggest first-order transitions.

GNO has two closely spaced anomalies at $T_{N1}(0)$ and $T_{N2}(0)$ and a third very small anomaly, of unknown origin, centered at $\sim 11 \text{ K}$ just below T_{N2} . There are several possible explanations for the presence of two transitions in GNO. One possibility is that they are associated with a transition from one kind of magnetic order to another, perhaps associated with the presence of weak single-ion anisotropy as has been observed in CsNiCl_3 .¹² [The small anomaly below $T_{N2}(0)$ might be a third transition related to an additional rearrangement of the ordered magnetic moments; it is also present with a reduced amplitude in C/T for 1 T but vanishes for $B > 1 \text{ T}$.] A second and more likely possibility, based on recent neutron-diffraction data¹³ for a single crystal, is that the two anomalies result because the kagome planes order

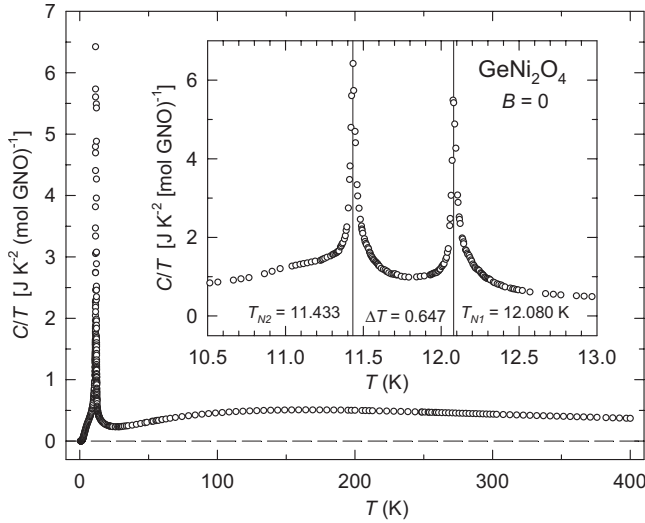


FIG. 2. C/T vs T for GNO in $B=0$ showing two closely spaced first-order antiferromagnetic transitions in the vicinity of 12 K where the $T_N(0)$ are defined by the maxima of the anomalies. A plot of C/T on an expanded temperature scale in the inset shows details of the double transition. Immediately above T_{N1} the C/T tail shown in the inset is a consequence of magnetic correlations.

first at T_{N1} and are followed by ordering on the triangular planes at T_{N2} —see Figs. 1 and 2. It is somewhat surprising, assuming this scenario is correct, that the entropy linked to each anomaly is nearly equal (see Sec. IV A) since the kagome lattice contains three times as many Ni^{2+} ions as the triangular lattice. Centered at ~ 5 K is a fourth anomaly, which is probably an anisotropy gap associated with the splitting of the $S=1$ ground state amplified by the antiferromagnetic-exchange interaction. Analysis of the low-temperature specific heat for $B=0$ shows it is associated with antiferromagnetic spin waves with an average gap of 10.9 K.

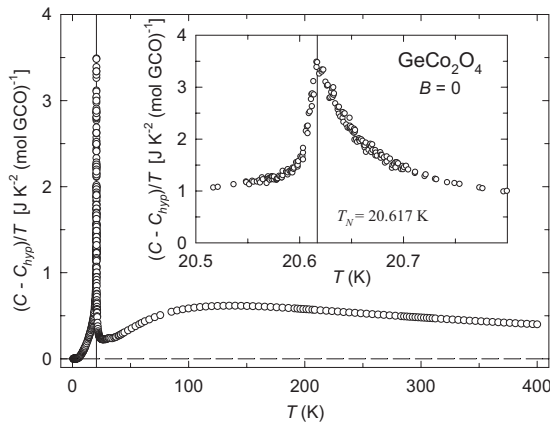


FIG. 3. $(C - C_{\text{hyp}})/T$ vs T for GCO in $B=0$ showing a single first-order antiferromagnetic transition in the vicinity of 20 K. A hyperfine specific-heat contribution for ^{59}Co has been subtracted—see Sec. IV B. The inset is a plot of $(C - C_{\text{hyp}})/T$ vs T near the transition on an expanded temperature scale showing details of the transition. The high-temperature $(C - C_{\text{hyp}})/T$ vs T tail immediately above T_N , shown in the inset, is related to magnetic correlations. T_N is defined by the anomaly maximum.

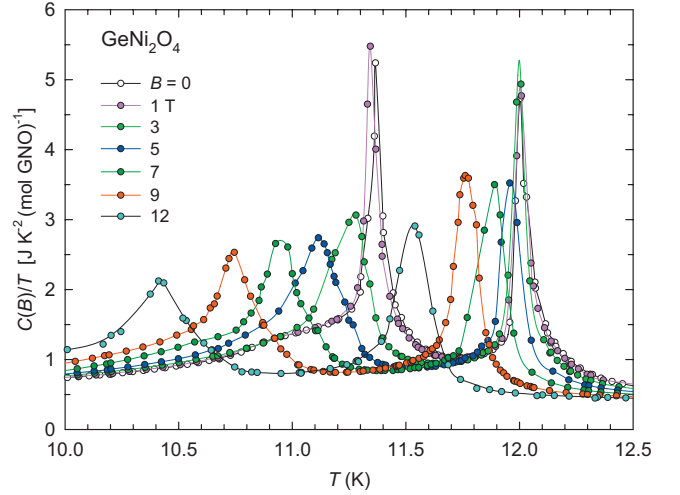


FIG. 4. (Color) $C(B)/T$ vs T in the transition region for GNO. For clarity the measurements at 14 T are not shown. Some of the transitions have maxima whose amplitudes do not decrease monotonically with increasing B , which is probably an artifact of the PPMS method of analysis for first-order transitions or because of an insufficient density of data in the region of the sharp transitions.

Surprisingly, concurrent with the gapped spin waves are ungapped spin waves. This could be additional evidence that the kagome and triangular planes order separately as suggested in Ref. 13. For both GNO and GCO, the entropy related to the anomalies at the Néel temperatures is $\sim 2\%$ of $2R \ln 3$ for each GNO anomaly and $\sim 3\%$ of $2R \ln 2$ for GCO—see Sec. IV.

2. Specific heats of GeNi_2O_4 in magnetic fields

Figure 4 is a plot of $C(B)/T$ vs T , and Fig. 5 is a plot of $C(B)/T$ vs T in the vicinity of $T_{N1}(B)$ and $T_{N2}(B)$, which shows the effect of increasing magnetic fields to 14 T on the transition anomalies. The broad anomaly in C/T vs T centered at ~ 11 K for $B=0$ and 1 T is suppressed for $B > 1$ T, but the 5-K anomaly is observed for all fields. In Fig. 6 $T_{N1}(B)$, $T_{N2}(B)$, and $T_{N1}(B) - T_{N2}(B)$ are plotted as a function of B . [$T_{N1}(B)$ and $T_{N2}(B)$ are defined as the maxima of the transitions.] Fields up to 14 T monotonically shift the transitions to lower temperatures while broadening and attenuating them. $T_{N2}(B)$ shifts more rapidly with increasing B than $T_{N1}(B)$ does until ~ 12 T, at which the decreases become approximately equal. As B increases the anomalies are broadened and attenuated. The shift to lower temperatures is consistent with antiferromagnetism and the somewhat greater sensitivity of T_{N2} to magnetic field is consistent with its identification as associated with the more weakly ordering triangular planes.¹³ The separations, $T_{N1}(B) - T_{N2}(B)$, increase with B and appear to approach a plateau at 14 T. Surprisingly, the shift of the anomalies to lower temperatures with increasing B is much smaller than for GCO, which has $T_N(0)$ approximately twice that of those for GNO—see Sec. III A 3. The magnetic fields do not split the ordering anomalies, which is an indication that GNO is magnetically isotropic.

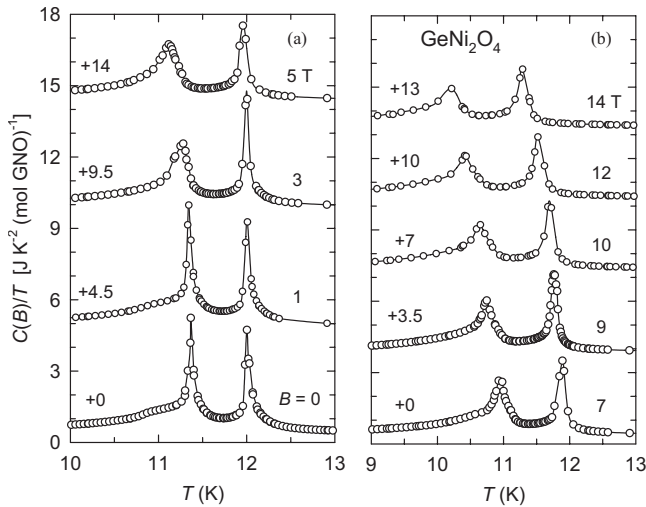


FIG. 5. $C(B)/T$ vs T in the vicinity of the $T_{N1}(B)$ and $T_{N2}(B)$ transitions, which illustrate the effect of magnetic fields on the antiferromagnetic transitions. For clarity the $C(B)/T$ vs T data are shifted vertically, relative to one another, by additive constants given in the figure. Curves through the data are guides to the eye. At $B=0$ and 1 T the broad maxima centered at ~ 11 K are apparent. This figure emphasizes the relatively small shift of the anomaly maxima to lower temperatures as B increases.

Above the transition region all $C(B)/T$ are convergent at ~ 30 K. This convergence, as well as the absence of any additional field-induced anomalies, is evidence that there is no hidden ordering or residual magnetic disorder in the ground state below 0.5 K for $B=0$. In magnetic fields any specific-heat anomaly linked to hidden ordering would be shifted to higher temperatures within the range of the measurements. If residual disorder is present in the ground state, the interaction of the disordered moments with the applied magnetic fields would increase the specific heats. Additional evidence to support this is the entropy balance between the $B=0$ and the $B>0$ specific-heat data at temperatures well above the transition region—see Sec. IV A. This entropy bal-

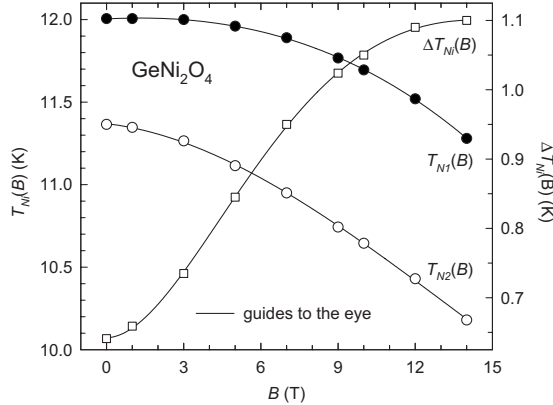


FIG. 6. $T_{N1}(B)$ (filled circles) and $T_{N2}(B)$ (open circles) are shown plotted as a function of magnetic field. They were determined using the $C(B)/T$ vs T maxima displayed in Fig. 5. The small increasing separation of the two anomalies (squares), $\Delta T_{Ni}(B) = T_{N1}(B) - T_{N2}(B)$, appears to be approaching a plateau for $B > 14$ T. (The subscript Ni is used to designate either N1 or N2.)

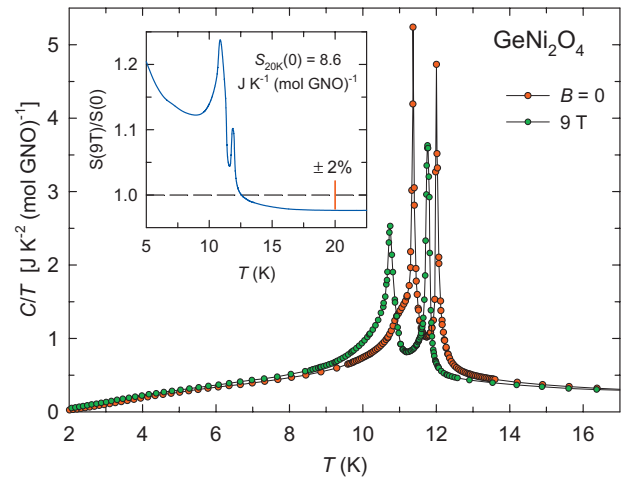


FIG. 7. (Color) $C(B)/T$ vs T for $B=0$ and 9 T, illustrating the entropy balance between the two fields. No contributions have been subtracted before evaluation of $S(B) = \int [C(B)/T] dT$ from 0 to 35 K. The inset shows the entropy ratio, $S(9\text{ T})/S(0)$. The ratio is unity to within $\pm 2\%$ as shown by the red bar at 20 K. All corresponding $S(B)/S(0)$ ratios are within this range, which is consistent with the expected accuracy of the PPMS.

ance and equality of the specific heats is illustrated in Fig. 7 for $B=0$ and 9 T. Section IV A contains analyses of the specific-heat data above the antiferromagnetic-ordering temperature to determine the lattice specific heat and, in the low-temperature region, to derive microscopic parameters and the magnetic entropy associated with the antiferromagnetic ordering.

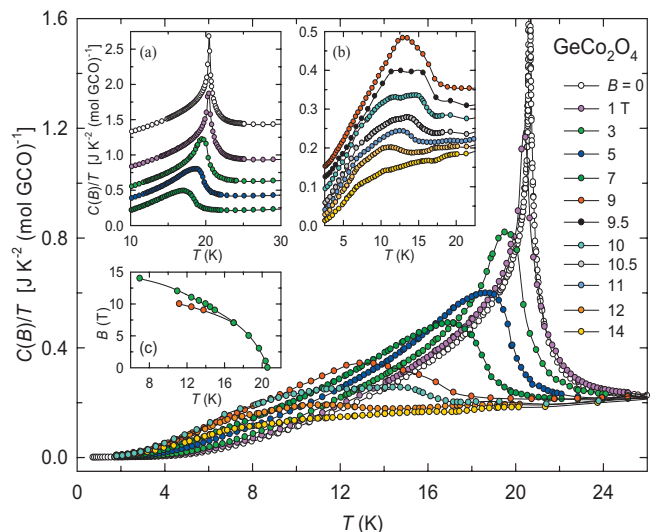


FIG. 8. (Color) $C(B)/T$ vs T for $0 \leq T \leq 30$ K. For clarity $C(B)/T$ are not shown for all B . No hyperfine contribution was observed except for $B=0$, since the lowest temperatures of the measurements for $B>0$ are only ~ 1.8 K. The C_{hyp}/T contribution for $B=0$ has been subtracted. The two insets of the figure, (a) and (b), show how the antiferromagnetic-ordering anomalies behave for all B . For clarity, the specific heats in different fields are displaced vertically. Inset (c) shows the loci of maxima of T for the specific-heat anomalies plotted as a function of magnetic field. The curves connecting the points are guides to the eye.

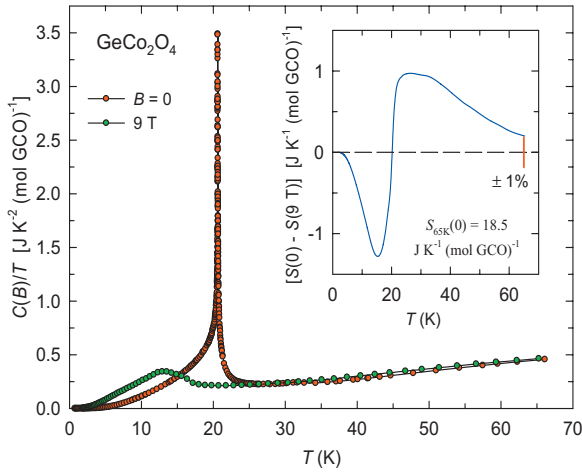


FIG. 9. (Color) $C(B)/T$ vs T for $B=0$ and 9 T illustrating the entropy balance between the two fields for GCO. Since the measurements extend only down to ~ 1.8 K, no hyperfine contributions were observed nor were corrections made. No specific-heat contributions have been subtracted before the evaluation of $S(B) = \int [C(B)/T]dT$. The inset shows the entropy difference between 0 and 9 T. The difference is zero to $\pm 1\%$ at 65 K as represented by the red bar. All of the $S(0) - S(B)$ fall within this $\pm 1\%$ range and $C(B)/T \approx C(0)/T$ at 65 K. These agreements are within the expected accuracy of the PPMS.

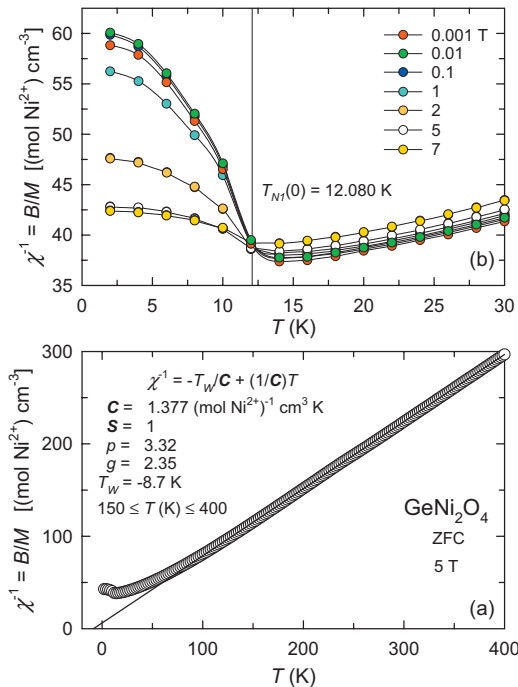


FIG. 10. (Color) (a): χ^{-1} vs T for GNO at 5 T over the experimental temperature range $2 \text{ K} \leq T \leq 400 \text{ K}$. The straight line through the data is a Curie-Weiss law fit for the temperature range $150 \text{ K} \leq T \leq 400 \text{ K}$. Fit parameters are tabulated in the figure. ZFC stands for “zero field cooled.” (b): $\chi^{-1}(B)$ vs T in the vicinity of the antiferromagnetic transitions for $0.001 \text{ T} \leq B \leq 7 \text{ T}$ —the range of the measurements.

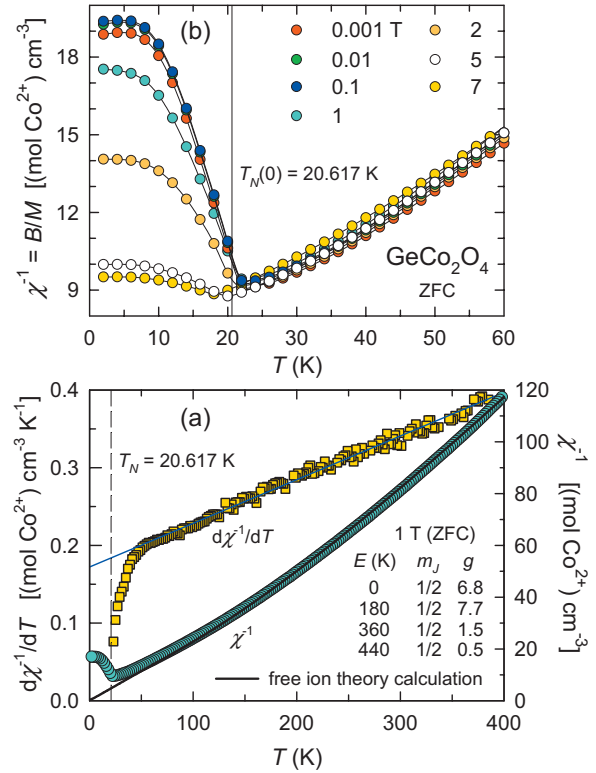


FIG. 11. (Color) (a): χ^{-1} vs T and the numerical derivative $d\chi^{-1}/dT$ vs T for 1 T for GCO. The derivative shows that the linear change in the curvature of χ^{-1} vs T , because of the higher-lying crystal-field levels, precludes the use of the Curie-Weiss law to extract parameters characterizing the ground state. The black curve is a fit of the χ^{-1} vs T data using the known crystal-field levels and free-ion theory [Eq. (1)], and it is a reasonably good representation for $T > 150$ K—see Sec. III B2. For $T < 400$ K crystal-field levels for $E > 440$ K make a negligible contribution to the susceptibility. Fit parameters are given in the figure. (b): $\chi^{-1}(B)$ vs T in the vicinity of the antiferromagnetic transitions in the range $0.001 \text{ T} \leq B \leq 7 \text{ T}$ —the magnetic-field range of the measurements.

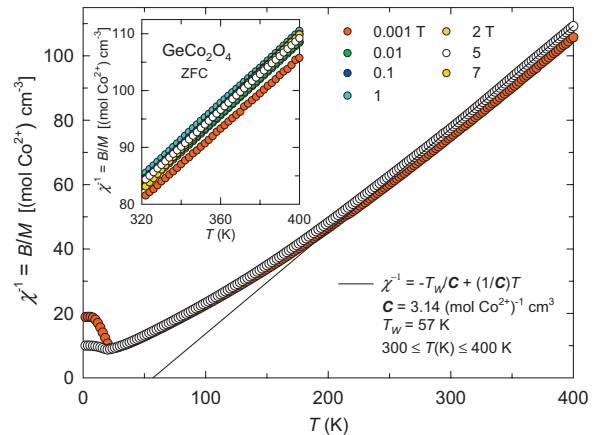


FIG. 12. (Color) χ^{-1} vs T for GCO for $B=0.001$ and 5 T. A Curie-Weiss fit in the range $300 \text{ K} \leq T \leq 400 \text{ K}$ for the 5 -T data is shown as the straight line in the figure and the fit parameters appear on the lower right.

3. Specific heats of GeCo_2O_4 in magnetic fields

Figure 8 is a plot of $C(B)/T$ vs T . The (a) and (b) insets show $C(B)/T$ vs T in the vicinity of the single transition at $T_N(B)$, which charts the evolution of the first-order transition with magnetic fields up to 14 T. As B is increased, the anomaly maxima shift to lower temperatures. Accompanying the shift is a broadening and attenuation until 14 T, at which the anomaly has become so broadened as to be virtually Schottky type. As the anomalies steadily decrease with increasing field, there is a compensating increase in the low-temperature specific heat, which is necessary to preserve the entropy balance of the system. This magnetic-field behavior is very different from that of GNO, i.e., a much larger $C(B)/T$ vs T maxima shift, broadening, and attenuation. However, similar to GNO, the monotonic shift in $T_N(B)$ to lower temperatures with increasing field is the anticipated behavior for antiferromagnetic ordering.

Insets (a) and (b) of Fig. 8 show $C(B)/T$ vs T in the vicinity of the anomalies on an expanded scale for all fields. Beginning at 9 T an asymmetry develops in the anomaly and from 9.5 to 10.5 T the anomalies are split. This splitting is probably related to the expected large magnetic anisotropy of the Co^{2+} ions. Since the sample is polycrystalline, the randomly oriented crystallites will have orientation-dependent interactions with B because of this anisotropy. For $B > 10.5$ T the splitting is not observed because of either the pronounced broadening of the anomalies in the higher fields and/or magnetic-domain alignment. The rapid broadening of the anomalies with increasing magnetic field is also explained by the anisotropy. Inset (c) shows the loci of the maxima of the anomalies.

For $B=9.5$ T there is a small broad feature centered at ~ 19 K that is probably related to the transition from cubic to tetragonal crystal symmetry. This crystal-structure transition is “uncovered” as the anomalies are shifted to lower temperatures. In 12 T the anomaly is shifted to ~ 17 K. This shift to lower temperatures with increasing magnetic fields is probably related to coupling between the magnetic moments and the lattice, which has been observed in single-crystal neutron-diffraction measurements.⁴ The area associated with the anomaly is small, attesting to a small enthalpy/latent heat (ΔH_{ct}) and entropy change (ΔS_{ct}) accompanying the lattice transition/distortion. An estimate of the anomaly’s area at 10.5 T gives $\Delta H_{\text{ct}} \sim 0.3$ J (mol GCO)⁻¹ and $\Delta S_{\text{ct}} \sim 0.015$ J K⁻¹ (mol GCO)⁻¹, which are $\sim 3\%$ of that associated with the antiferromagnetic transition—see Fig. 8(b).

Above the transition region all $C(B)/T$ vs T are convergent at ~ 65 K. As in GNO this convergence, as well as the absence of any additional field-induced anomalies at low temperatures, is verification that no hidden ordering or residual magnetic disorder in the ground state exists below 0.5 K for $B=0$. Additional proof for no hidden ordering or magnetic disorder is the entropy balance between the $B=0$ and the $B>0$ specific heats at temperatures well above the transition region—see Sec. IV B. This entropy balance and the equality of the specific heats well above T_N is illustrated in Fig. 9 for $B=0$ and 9 T.

B. Magnetic susceptibility

Magnetic-susceptibility measurements can be used to gain an additional insight into the antiferromagnetic ordering of the two spinels. The Curie-Weiss law, $\chi=C/(T-T_W)$, where $C=N_A g^2 S(S+1)\mu_B^2/3k_B$ (with N_A as Avogadro’s number, μ_B as the Bohr magneton, g as the spectroscopic-splitting factor, and k_B as the Boltzmann constant), and the effective number of Bohr magnetons, $p=g[S(S+1)]^{1/2}=2.828C^{1/2}$, is used to interpret the data for GNO but not for GCO because of the relatively close proximity of crystal-electric-field states to the ground state. When fitting χ it is assumed that any temperature-independent magnetism (χ_0) is negligibly small.

1. GeNi_2O_4 magnetic susceptibility and analysis

Figure 10(a) is a plot showing χ^{-1} vs T over the range of the measurements for 5 T. The straight line through the points is a Curie-Weiss law fit in the range $150 \text{ K} \leq T \leq 400$ K. Parameters from the fit are given in the figure.

Figure 10(b) illustrates the evolution of $\chi^{-1}(B)$ vs T as B is increased in the region of the antiferromagnetic ordering. On the scale used for the plot, the χ^{-1} vs T measurements show no indication of the double transition observed in the specific heat. However, χ measurements at more closely spaced temperatures for $B=0.01$ T do show both transitions.⁵ The plots of $\chi^{-1}(B)$ vs T increase monotonically with B above $T_{N1}(B)$. Below $T_{N1}(0)$ monotonic increases in $\chi^{-1}(B)$ vs T are observed for $B=0.001-0.01$ T. For $B > 0.01$ T there is a monotonic decrease. This evolution of $\chi^{-1}(B)$ vs T with magnetic field is probably related to the alignment of magnetic domains with B .

A Curie-Weiss law fit shown in Fig. 10(a) for 5 T has $T_W=-8.7$ K, where the negative value indicates antiferromagnetism with a value close to the observed $T_{N1}(0)=12.080$ K obtained from the specific-heat measurements. The ratio $|T_W/T_{N1}(0)|=0.7$, near unity, indicates an absence of frustration.¹⁴ However, there are deviations of χ^{-1} vs T from the Curie-Weiss behavior below ~ 125 K, which indicate that substantial magnetic correlations begin to develop well above the Néel transition. From the Curie-Weiss fit the effective number of Bohr magnetons is $p=3.32$, which is in the range usually found for Ni^{2+} ions in octahedral crystal electric fields.² Using $p=3.32$ allows a value for g to be calculated for $S=1$ from the relationship $p=g[S(S+1)]^{1/2}$. The result, $g=2.35$, is greater than the spin-only value of 2. This is due to the second-order perturbation, between the $^3A_{2g}$ ground state and the $^3T_{2g}$ excited crystal-field state, introduced by spin-orbit coupling.¹⁵ This leads to mixing of the $^3A_{2g}$ and $^3T_{2g}$ levels and thereby introduces orbital character into the ground state, which increases the g value. In the presence of a trigonal field, in addition to the cubic field, the same mechanism leads to a zero-field splitting of the ground state since the $^3T_{2g}$ excited state is split in first order by the trigonal field and these split levels are then spin-orbit coupled in second order to the ground state.¹⁵ This also introduces some anisotropy into the Ni^{2+} g value.

2. GeCo_2O_4 magnetic susceptibility and analysis

Figure 11(b) is a plot of $\chi^{-1}(B)$ vs T for $B=0.001$ and 5 T over the temperature range $2 \text{ K} \leq T \leq 400$ K. For B

>0.001 T, $\chi^{-1}(B)$ vs T is the same to within experimental accuracy and the $\sim 3\%$ difference at 400 K for 0.001 T can be accounted for if there is an uncertainty in the field of $\sim 3 \times 10^{-5}$ T. The inset of Fig. 11(b) shows $\chi^{-1}(B)$ vs T in the range $320 \text{ K} \leq T \leq 400 \text{ K}$ for all B . While χ^{-1} vs T for GNO is linear over a wide range of temperatures— $150 \text{ K} \leq T \leq 400 \text{ K}$ at 2 and 5 T— χ^{-1} vs T for GCO is curved with *no linear range* below 400 K. This is clearly shown in Fig. 11(a), where χ^{-1} vs T and the derivative $d\chi^{-1}/dT$ vs T are plotted for $B=1$ T. The curvature is a result of the higher crystal-field Kramers doublets, and the Curie-Weiss law is inapplicable if χ has temperature-dependent contributions from such energy levels above the ground state. Instead, the Van Vleck susceptibility must be calculated based upon knowledge of the energies and wavefunctions for the excited states. When such higher levels are present, the Curie-Weiss law can be used only at temperatures where the higher-lying states make a negligible contribution, which is not possible for GCO since $T_N(0)=20.617$ K.

Although the Curie-Weiss law cannot be used to determine the sign or strength of the magnetic exchange for GCO, other investigators^{16,17} did so and reported a positive T_W instead of the negative one expected for antiferromagnetic interactions. Over limited temperature intervals, χ^{-1} vs T is approximately linear and relatively good fits to the Curie-Weiss law are possible. However the derived parameters are not valid. Figure 12 shows such a fit to the 5 T data for $300 \text{ K} \leq T \leq 400 \text{ K}$ with a $T_W=57$ K, indicating ferromagnetic interactions, which contradicts the experimentally observed antiferromagnetism. (Fits over different intervals give different values of T_W . For example, in Ref. 16 a fit of χ^{-1} vs T in the range $300 \text{ K} \leq T \leq 800 \text{ K}$ has a $T_W=81$ K, while in Ref. 17 a fit in the range $180 \text{ K} \leq T \leq 300 \text{ K}$ gave $T_W=40$ K.) The positive values of T_W are a result of the curvature of χ^{-1} vs T [see Fig. 11(a)], which is related to the presence of the crystal-field states not far removed from the ground state.

In order to extract the exchange contribution to the Weiss temperature, it is first necessary to subtract the influence of the excited crystal-field levels. This could be accomplished, for example, by measuring the magnetic susceptibility of Co^{2+} in a structurally identical but magnetically dilute lattice where the exchange contributions are eliminated and only the crystal-field contribution remains. Such measurements have not yet been reported for GeCo_2O_4 since an appropriate nonmagnetic analog into which small quantities of Co^{2+} can be doped has not been identified.

If the Co^{2+} magnetic moments in GCO are free and the spacing of the crystal-field Kramers doublet levels with their corresponding g and m_J values known, the magnetic moment (M) can be calculated to first-order using the expression

$$M = \frac{-N_A \sum_{i=0}^5 \sum_{m_J=-1/2}^{1/2} g_i m_J \mu_B e^{-(E_i + g_i m_J \mu_B B)/RT}}{\sum_{i=0}^5 \sum_{m_J=-1/2}^{1/2} e^{-(E_i + g_i m_J \mu_B B)/RT}}. \quad (1)$$

In Eq. (1), i is an index designating the six Kramers doublets with components m_J , taken as $\pm 1/2$ pairs, and E_i is the

separation of the i th level from the ground state ($i=0$, $E_0=0$), μ_B is the Bohr magneton, R is the gas constant, and N_A is Avogadro's number. Since the $g_i m_J$ always occur as a product designating m_J as a $\pm 1/2$ doublet makes g_i a fictitious spectroscopic-splitting factor whose value is determined from both spin and orbital contributions. (At the present time the g_i are not known from either experiment or theory for GCO.) In Fig. 11(a) is a plot of the experimental data for $B=1$ T with a fit using Eq. (1) shown as the black curve. The two crystal-field levels at 1760 and 1930 K make a negligible contribution to χ^{-1} below 400 K and are not included in the fit. The parameters from the fit are tabulated in the figure. This simplistic approach provides a relatively good fit, which demonstrates that the low-lying crystal-field levels contribute to the curvature in χ^{-1} vs T . However, the value of g_0 is larger than theoretically expected, assuming $m_J = \pm 1/2$ for a Co^{2+} ion in a large trigonal crystal field, for a polycrystalline sample.¹⁸ Since there are also higher-order coupling interactions between the ground state and excited crystal-field levels that will contribute to the magnetic moment, the first-order expression [Eq. (1)] is only an approximation and, although the fit is relatively good, the g_i parameters are empirical.⁴ In addition, there are undoubtedly interactions between the Co^{2+} ions (i.e., substantial magnetic correlations) that are also not accounted for by Eq. (1).

The large ground-state g value obtained for GCO suggests that the trigonal field is important and that the ground-state Kramers doublet derives from the 4E_g orbital doublet [see Fig. 4 of Ref. 18]. This form of single-ion anisotropy is reminiscent of that observed in pyrochlore spin ices in that the Co^{2+} spins should point into, or out of, the tetrahedra. It should also lead to an Ising behavior for the Co^{2+} ions. Thus, we would expect that at low temperatures GCO is in the universality class of a three-dimensional (3-D) Ising antiferromagnet.

Figure 11(b) illustrates the evolution of $\chi^{-1}(B)$ vs T as B is increased in the magnetic-ordering region. There is a monotonic increase in $\chi^{-1}(B)$ vs T with B above T_N . Below $T_N(0)$ from $B=0.001$ to 0.1 T, there is an increase in $\chi^{-1}(B)$ vs T followed by a monotonic decrease as B increases. This evolution of $\chi^{-1}(B)$ vs T with magnetic field is probably related to magnetic-domain alignment with increasing B . The plots shown in Fig. 11(b) are very similar to those in Fig. 10(b) for GNO.

IV. SPECIFIC-HEAT ANALYSIS FOR ZERO MAGNETIC FIELD

In this section the specific heats for GNO and GCO are analyzed to evaluate the lattice contribution, a first step needed to enable a determination of the magnetic specific heat (C_{mag}), which allows a numerical evaluation of the magnetic entropy (S_{mag}) associated with the antiferromagnetic ordering. Parameters related to the ordering (e.g., antiferromagnetic spin waves and energy gaps) are derived from fits to the low-temperature specific heat where the lattice contribution is negligible.

The harmonic-lattice approximation is used to evaluate the magnetic-field-independent lattice specific-heat (C_{lat}) contribution:

$$C_{\text{lat}} = B_3 T^3 + B_5 T^5 + B_7 T^7 + \dots \quad (2)$$

An alternative method uses a sum of Debye and Einstein functions—an application of the Blackmann theory¹⁹—to represent the 3 acoustic and 18 optical modes of the lattice well above T_N . Both methods were used in the analysis given in Ref. 5 and the derived magnetic entropies obtained by evaluating $\int[(C - C_{\text{lat}})/T]dT$ were essentially identical. The specific heat related to crystal-field levels (C_{cf}) can be represented by a Schottky function for a set of unevenly spaced energy levels:

$$\frac{C_{\text{cf}}}{R} = \frac{\sum_{i=1}^j d_i (E_i/T)^2 e^{-E_i/T} \sum_{i=1}^j d_i (E_i/T) e^{-E_i/T}}{d_0 + \sum_{i=1}^j d_i e^{-E_i/T}}, \quad (3)$$

where the E_i are the j crystal-field levels, d_i is the E_i level degeneracy, and d_0 is the ground-state degeneracy.

For the magnetic correlations immediately above T_N , the expansion representing the “tail” of the specific-heat contribution (C_{mc}) is given by the usual representation:

$$C_{\text{mc}} = \sum_{i=2}^m A_i/T^i, \quad (4)$$

where the summation is for $i=2,3,4,\dots,m$ for as many terms as necessary depending on the lower-temperature range of the fit.

Hyperfine contributions to the specific heat (C_{hyp}) are represented by the first term of the high-temperature expansion of a Schottky function:

$$C_{\text{hyp}} = \sum_{i=1}^k D_i/T^2, \quad (5)$$

where the summation is over the k ions with a nuclear moment. In the absence of a nuclear quadrupole contribution,

$$\frac{D}{R} = \frac{(I+1)}{3I} \left(\frac{\mu B_n}{k_B} \right)^2, \quad (6)$$

where R is the gas constant, I is the nuclear spin, μ is the nuclear moment in units of the nuclear magneton (μ_n), B_n is the magnetic hyperfine field at the nucleus, and k_B is the Boltzmann constant. For GNO and GCO the nuclei with magnetic moments are: (1) ^{73}Ge (7.73% abundance), with $I=9/2$ and $\mu=-0.880\mu_n$; (2) ^{61}Ni (1.14% abundance), with $I=3/2$ and $\mu=-0.750\mu_n$; and (3) ^{59}Co (100% abundance), with $I=7/2$ and $\mu=4.627\mu_n$. For the range of temperatures used in the measurements reported here, only ^{59}Co makes a measurable hyperfine contribution to the specific heat.

When a band of closely spaced ground-state levels is split with a gap (Δ_x), there will be a specific-heat contribution (C_x) associated with excitations from the lower to the upper band that is analogous to what happens in a superconductor. This C_x contribution can be represented, at sufficiently low temperatures, by the exponential expression

$$C_x = B_x T^n e^{-\Delta_x/T}, \quad (7)$$

where n is either empirically determined from the fit or calculated theoretically.

Below T_N antiferromagnetically ordered magnetic moments will have spin-wave excitations whose specific heat C_{af} in the low-temperature region for $T < \sim T_N/3$ is represented by Eq. (7) recast in the form

$$C_{\text{af}} = B_{\text{af}} T^n e^{-\Delta_{\text{af}}/T}, \quad (8)$$

where n is either empirically determined by fixing it at positive and negative integers and selecting the value that has an rms minimum or calculated theoretically, and Δ_{af} is a gap in the spin-wave spectrum. For ungapped antiferromagnetic spin waves, Eq. (8) becomes

$$C_{\text{af}} = B_{\text{af}} T^3. \quad (9)$$

A T^3 term in the expressions for both the lattice and isotropic spin waves complicates the separation of their contributions since only the composite term $\beta_3 T^3 = (B_3 + B_{\text{af}}) T^3$ is determined from a low-temperature fit. In that situation B_3 must be evaluated above T_N . Usually $B_{\text{af}} \gg B_3$. Some useful books related to the analysis of specific-heat and magnetic-susceptibility data are given in Ref. 20.

A. Specific-heat analysis for GeNi_2O_4

The magnetic specific heat C_{mag} is obtained from a two-step analysis of the data for $T < T_{N2}$ and $T > T_{N1}$. The analysis is made for the BYU specific-heat measurements for $B=0$. Above T_{N1} the fitting expression is $C = \sum A_m/T^m + \sum B_n T^n$, where $\sum A_m/T^m$ ($m=2,3,4,\dots$) is the semiempirical representation, Eq. (4), for the magnetic correlations and $C_{\text{lat}} = \sum B_n T^n$ ($n=3,5,7,9,\dots$) is the harmonic-lattice approximation, Eq. (2). From $14 \text{ K} \leq T \leq 75 \text{ K}$ the data are fitted with $m=2,3,4$ and $n=3,5,7,9,11$. (Since the first crystal-field multiplet above the ground state is at $\sim 12\,400 \text{ K}$, no provision for a C_{cf} contribution is necessary.) The fit is good with an rms of 0.3% with $B_3 = 2.38 \times 10^{-4} \text{ J K}^{-4} (\text{mol GNO})^{-1}$ and $\Theta_D = 386 \text{ K}$. (The calculation of Θ_D uses the expression $\Theta_D = (12\pi^4 R N_a / 5 B_3)^{1/3}$, where R is the gas constant and N_a is the number of atoms per formula weight.) Figure 13 is a plot of the data in the high-temperature region above $T_{N1}(0)$ where the curve represents the fit.

For $T < T_{N2}$, a plot of C/T vs T^2 does not have the low-temperature region of linearity expected for $C/T = B_3 T^2$. Instead, there is a broad anomaly (centered at $\sim 5 \text{ K}$), which implies the presence of another component in addition to those expected for the lattice and ungapped antiferromagnetic spin waves—see the inset of Fig. 14. The 5-K anomaly suggests the presence of an energy gap. Inelastic-neutron-scattering spectroscopy shows that the gap is temperature dependent and vanishes as $T \rightarrow T_{N1}(0)$ —see Fig. 15. The inelastic-neutron-scattering results shown in Fig. 15 are consistent with gapped spin waves originating from the single-ion anisotropy of the $S=1$ ground-state multiplet and the exchange interaction. In addition to the gapped spin waves the analysis, described below, demonstrates there are un-

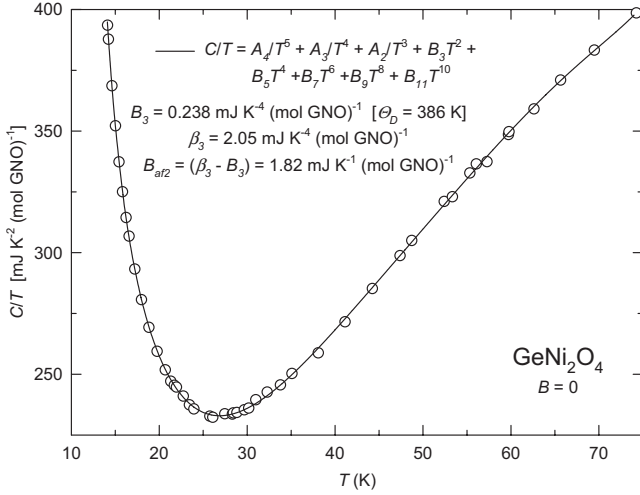


FIG. 13. C/T vs T for GNO above T_{N1} for $B=0$. The data are fitted to the expression given in the figure and described in Sec. IV A.

gapped spin waves as well, which suggests two different kinds of antiferromagnetic ordering for the Ni^{2+} ions.

A good fit to the data for $T \leq 6$ K is obtained with an rms of 0.5% using a least-squares procedure with the expression $C = \beta_3 T^3 + B_{af1} T^n e^{-\Delta_{af1}/T}$, where $\beta_3 = (B_3 + B_{af2})$ and Eq. (8) for gapped spin waves is used to fit the data in the vicinity of the 5-K anomaly. By holding n fixed at positive and negative integers, a minimum rms is found for $n=0$; and a fit with n included as a variable gives 0.09. The parameters, fixing $n=0$, are $\beta_3 = 2.05 \times 10^{-3} \text{ J K}^{-4} (\text{mol GNO})^{-1}$, $B_{af1} = 8.97 \text{ J K}^{-1} (\text{mol GNO})^{-1}$, and $\Delta_{af1} = 10.9 \text{ K}$, which is confirmed by inelastic-neutron-scattering measurements—see Fig. 15. (We have arbitrarily assumed that the gap is associ-

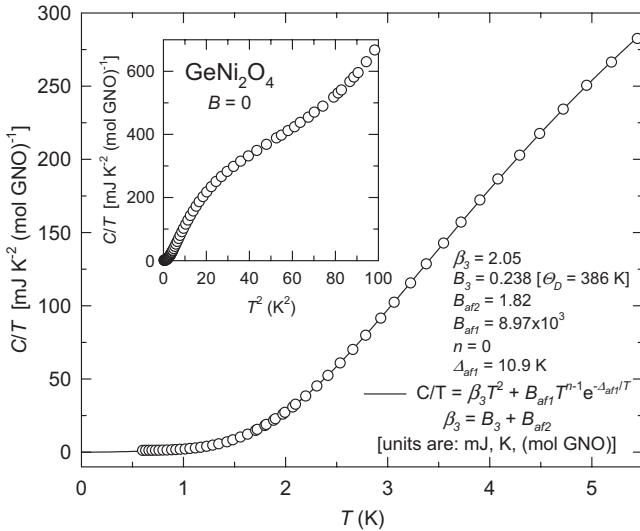


FIG. 14. C/T vs T below T_{N2} for $B=0$ for GNO. Below T_{N2} the data are fitted to the expression given in the figure using a least-squares procedure for $T < 6$ K, as described in Sec. IV A. The inset shows the broad anomaly in C/T vs T^2 that is postulated to be due to a spin-wave gap Δ_{af1} . For an explanation of these data, see Secs. IV A and VI D. Note: β_3 , B_3 , and B_{af2} are in units of $\text{mJ K}^{-4} (\text{mol GNO})^{-1}$; B_{af1} is in units of $\text{mJ K}^{-1} (\text{mol GNO})^{-1}$.

ated with T_{N1} .) Since the inelastic-neutron-scattering measurements have a gap that is temperature dependent, the $\Delta_{af1} = 10.9 \text{ K}$ derived from the fit to the specific-heat data is an average. From B_3 , from the fit above T_{N1} , the ungapped spin-wave parameter $B_{af2} = 1.82 \times 10^{-3} \text{ J K}^{-4} (\text{mol GNO})^{-1}$. Figure 16 is a plot of $\ln(C - \beta_3 T^3)$ vs $1/T$, which is linear to $\sim 6 \text{ K}$ ($\sim 1/2 T_{N2}$) and represents the contribution to the low-temperature specific heat related to the $\Delta_{af1} = 10.9 \text{ K}$ gap. The magnetic moments of the Ni^{2+} ions in GNO are essentially spin only and are expected to have spin waves that are isotropic. However, the concurrent presence of both gapped and ungapped spin waves is surprising in a cubic material where all the Ni^{2+} ions are equivalent, at least in the paramagnetic phase. This could be understood if the kagome and triangular planes order separately, as claimed by the authors of Ref. 13, who used their results to explain the double-peaked ordering.

A theoretical approximation for the specific heat for ungapped spin waves²¹ is $C_{af} = c_{af} R [RT / (2SJ)]^3$, where J is the exchange energy and c_{af} is a constant related to the lattice symmetry. By setting $C_{af} = B_{af} T^3$, the equation can be rearranged to $J = (R^{4/3} / 2S) (c_{af} / B_{af})^{1/3}$, where $c_{af} = 0.028$ for an fcc lattice. If the ungapped spin waves are linked with either the kagome or triangular planes, $B_{af} = 4/3 (B_{af2} / 2)$ or $4 (B_{af2} / 2)$, respectively, to account for the number of Ni^{2+} associated with each and to normalize J to 1 mol of Ni^{2+} per plane. $J_K = 24 \text{ J} (\text{mol Ni}^{2+})^{-1}$ (2.9 K or 0.25 meV) for kagome planes and $J_T = 17 \text{ J} (\text{mol Ni}^{2+})^{-1}$ (2.0 K or 0.18 meV) for the triangular planes. We do not know with which plane to associate the T^3 term in the magnetic specific heat.

An estimate of an overall J_{KT} can also be calculated using $T_W = -8.7 \text{ K}$ from the Curie-Weiss law fit to the magnetic-susceptibility data. From the mean-field expression²² $J = [3T_W / (zS(S+1))]$, where the number of nearest neighbors $z=6$, $J_{KT} = 2.2 \text{ K}$ [0.19 meV or 18 J $(\text{mol Ni}^{2+})^{-1}$], which is in reasonable agreement with the values estimated from the ungapped spin-wave specific heat given above.

The exchange energy J can be used to show that sufficiently strong magnetic fields will reduce disorder in the ground state. In magnetic fields the energy scale, represented by μB , becomes comparable to the exchange energy, $J \sim 20 \text{ J} (\text{mol Ni}^{2+})^{-1}$, for $B = 4 \text{ T}$ for which $\mu B = 22 \text{ J} (\text{mol Ni}^{2+})^{-1}$. This implies that disorder in the ground state would be altered for $B > 4 \text{ T}$ with corresponding increases in the specific heats and entropies compared with the $B=0$ values. Such increases are not observed in magnetic fields up to 14 T and there is no evidence to support the presence of ground-state disorder.

The specific heats in constant magnetic fields, measured at LANL, for $T \leq 4 \text{ K}$ are shown in Fig. 17. (For $B=0$ they differ by as much as $\pm 3\%$ from the BYU measurements but are within the expected experimental accuracy of the PPMS.) As B increases there is a monotonic increase in $C(B)$. Component specific heats for the lattice and the gapped and ungapped spin waves are shown as curves in the figure for $B=0$, where the gapped component dominates. It is unreasonable to expect that either $C_{af1}(B)$ or $C_{af2}(B)$ will have the same temperature dependence for $B > 0$ as they do for $B=0$.

The magnetic entropy S_{mag} is obtained by a numerical evaluation of the $\int [(C - C_{\text{lat}}) / T] dT$ in the range $0 \text{ K} \leq T$

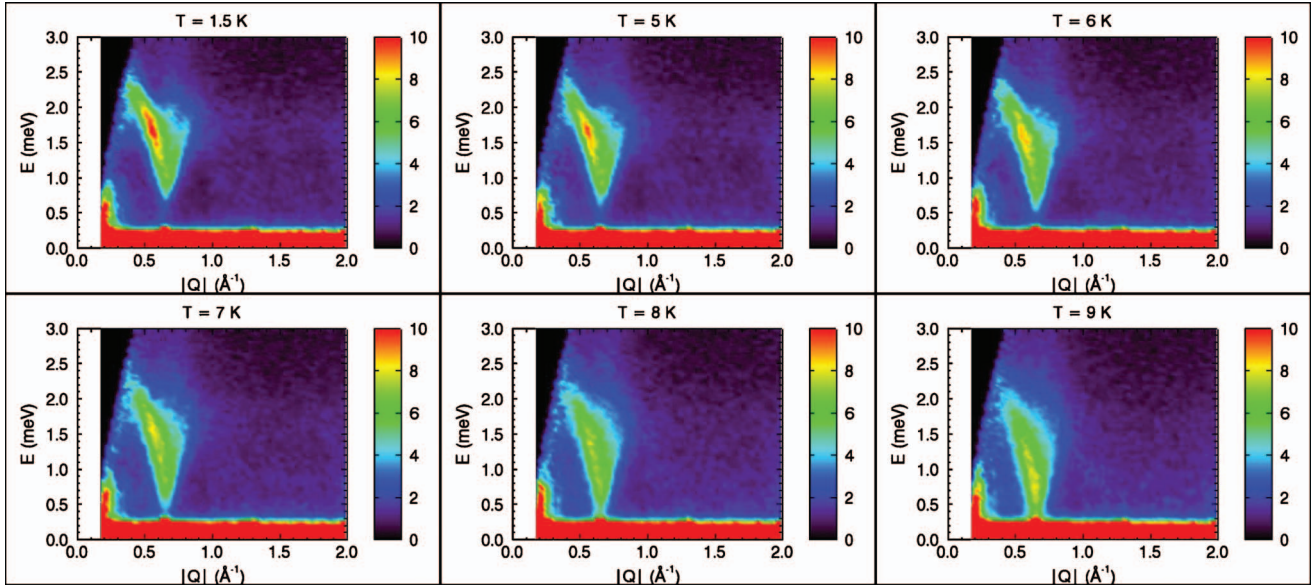


FIG. 15. (Color) Inelastic-neutron-scattering spectrum for polycrystalline GNO measured at temperatures in the range $1.5 \text{ K} \leq T \leq 9 \text{ K}$ using the disk chopper spectrometer (Ref. 11) at the NIST Center for Neutron Research. The incident-neutron wavelength was 3.2 \AA . At the antiferromagnetic wave vector $Q=0.65 \text{ \AA}^{-1}$, there is an energy gap at 1.5 K in the magnetic excitations of $E \sim 0.8 \text{ meV}$ ($\sim 9 \text{ K}$). As the temperature is increased, the gap decreases and vanishes as $T \rightarrow T_N$. For $Q \leq 2.0 \text{ \AA}^{-1}$ there is no indication of the gapless spin waves derived from the fit to the low-temperature specific-heat data—see Sec. IV A and Fig. 16.

$\leq 75 \text{ K}$ plus the contribution from 75 K to ∞ , which is assumed to be $(A_2/3T^3 + A_3/4T^3 + A_4/5T^4)$ evaluated at 75 K —see Fig. 14. In Fig. 18, C_{mag}/T vs T and S_{mag} vs T are plotted for $B=0$; the inset shows S_{mag} vs T , on an expanded scale, in the vicinity of T_{N1} and T_{N2} . The entropy recovered from the magnetic specific-heat analysis is $S_{\text{mag}} = 10.33 \text{ J K}^{-1} (\text{mol GNO})^{-1}$. Of this $\sim 5.2 \text{ J K}^{-1} (\text{mol GNO})^{-1}$ is recovered below T_{N1} and

$\sim 5.1 \text{ J K}^{-1} (\text{mol GNO})^{-1}$ above T_{N1} , which is $\sim 50\%$ for each region. At the two first-order transitions the entropies related to the anomalies are 0.367 and $0.330 \text{ J K}^{-1} (\text{mol GNO})^{-1}$ at T_{N1} and T_{N2} , respectively—see the inset of Fig. 18. The related enthalpies (latent heats) at the two transitions are $\Delta H_1 = 4.45 \text{ J} (\text{mol GNO})^{-1}$ and $\Delta H_2 = 3.78 \text{ J} (\text{mol GNO})^{-1}$.

If the ground state of Ni^{2+} in GNO has $S=1$, the associated entropy of ordering is $2R \ln(2S+1)$

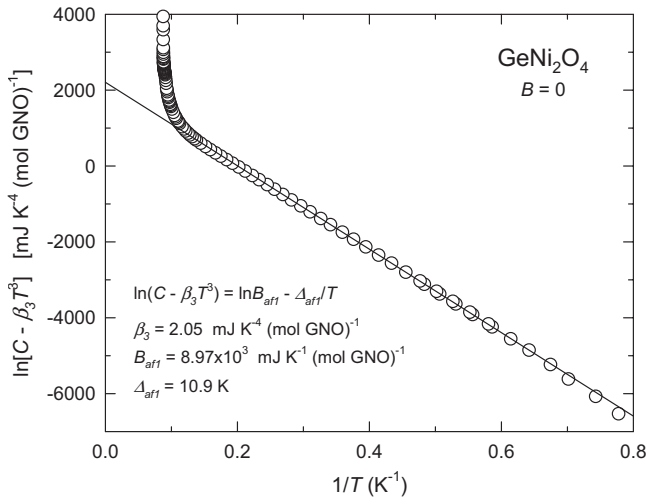


FIG. 16. This plot illustrates the exponential nature of the specific heat following subtraction of $\beta_3 T^3 = (B_3 T^3 + B_{\text{af}2} T^3)$. It demonstrates consistency with the expression $C_{\text{af}1} = B_{\text{af}1} e^{-\Delta_{\text{af}1}/T}$ for gapped antiferromagnetic spin waves, which is valid up to $\sim 6 \text{ K}$ ($\sim 1/2T_{N2}$). There is scatter in the data below $\sim 1.25 \text{ K}$ that increases as T decreases. After subtraction of $\beta_3 T^3$ the contribution to $C_{\text{af}1}$ below $\sim 1.25 \text{ K}$ is essentially zero; the small, scattered residuals are, in effect, equal to the experimental measurement errors.

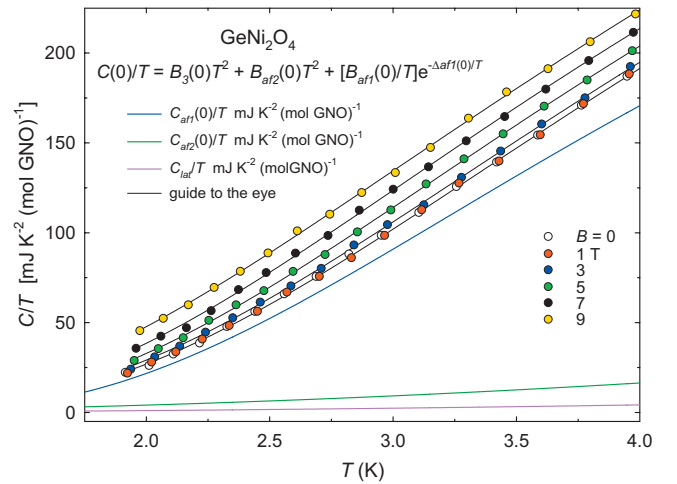


FIG. 17. (Color) Plots of $C(B)/T$ vs T are shown in magnetic fields up to 9 T . Curves through the data are guides to the eye. The C_{lat}/T component is shown as the pink curve. For $B=0$ the $C_{\text{af}2}/T$ vs T and $C_{\text{af}1}/T$ vs T components are shown as the green and blue curves, respectively. Their contributions are in the sequence $C_{\text{af}1}(0)/T \gg C_{\text{af}2}(0)/T > C_{\text{lat}}/T$, whose order probably persists for $B > 0$. For $B > 0$ there is no simple analytical model to fit the data such as the expression for $B=0$ shown in the figure—see Sec. IV A.

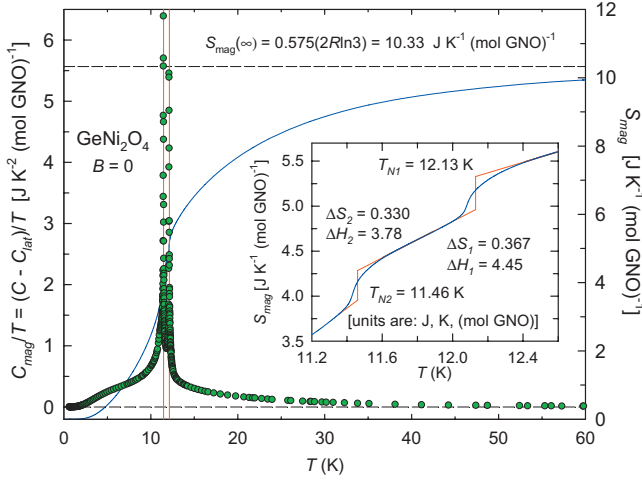


FIG. 18. (Color) Shown in this figure is a plot of C_{mag}/T vs T , obtained by subtracting C_{lat}/T , and that of S_{mag} vs T calculated by numerical evaluation of $\int (C_{\text{mag}}/T)dT$ for $B=0$. The anomaly associated with the anisotropic antiferromagnetic spin waves is clearly visible and is centered at ~ 5 K. In the inset S_{mag} is shown on an expanded temperature scale in the vicinity of the transitions. The entropy-conserving constructions provide an accurate determination of T_{N1} and T_{N2} in lieu of the definition using the maxima in C/T that are larger but differ by <0.05 K. Those constructions also provide a means of determining the enthalpy and entropy for the first-order transitions whose values are tabulated in the inset. Note: The units of S are $\text{J K}^{-1} (\text{mol GNO})^{-1}$ and of H are $\text{J} (\text{mol GNO})^{-1}$.

$=18.27 \text{ J K}^{-1} (\text{mol GNO})^{-1}$, but only 56.5% of this is recovered. Two obvious possibilities to account for this missing entropy are hidden ordering below the lowest temperature of the measurements and/or low-temperature disorder in the ground state induced by frustration. If either or both of these possibilities is true, the specific-heat measurements in magnetic fields would have Schottky-type anomalies for any hidden ordering that would be observed as they move to higher temperatures with increasing B . For magnetic disorder the in-field specific heats would be increased. The analysis shown in Fig. 7 proves that neither of these cases can account for the entropy discrepancy. Well above T_{N1} for $B=0$ and 9 T, the entropies are the same to within the measurement accuracy and the specific heats for $B=0$ and 9 T are equal. Another possibility, which could explain the missing entropy, is the presence of significant magnetic correlations at temperatures above 75 K, which currently appears to be the more likely explanation—see Sec. VI C.

Note that $T_N(B)$ throughout the paper are defined as T at the maxima in the $C(B)/T$ anomalies. Entropy-conserving constructions shown in the inset of Fig. 18 have $T_N(0)$ that are slightly larger than the $T_N(0)$ defined by the maxima in $C(0)/T$. Those $T_N(0)$ in the Fig. 18 inset are more nearly correct. However, the differences are not large (<0.05 K) and $T_N(B)$ will continue to be defined in the paper as T at the maximum in $C(B)/T$.

B. Specific-heat analysis for GeCo_2O_4

In contrast to the case of GNO, obtaining an analytical representation for the lattice specific heat of GCO is compli-

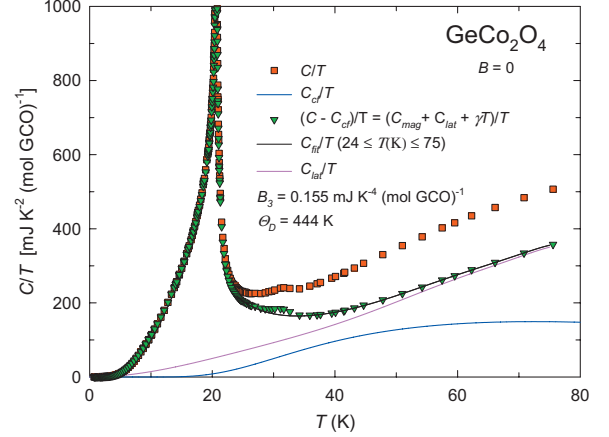


FIG. 19. (Color) For $B=0$ C/T vs T for GCO are shown as red squares. Unlike GNO the crystal-electric-field states for GCO make a contribution to the specific heat, C_{cf} , in the temperature range of the measurements and the blue curve represents that contribution. The C_{cf} specific heat is subtracted from C and $(C-C_{\text{cf}})/T$ vs T is shown as the green triangles. These corrected data are fitted using the expression given in Fig. 13 for GNO plus a γT term and use the same fitting procedure, as described in Sec. IV B. The fit is represented by the black curve; the pink curve represents $C_{\text{lat}}/T = (C-C_{\text{mag}}-C_{\text{cf}}-\gamma T)/T$.

cated by the presence of crystal-electric-field levels. The Co^{2+} free-ion state, $^4F_{9/2}$, in GCO is split into six Kramers doublets by a combination of crystal-electric-field interactions and spin-orbit coupling.⁴ These states contribute to the specific heat C_{cf} in the temperature region above T_N where C_{lat} is determined. Equation (3) is used to calculate C_{cf} , as-

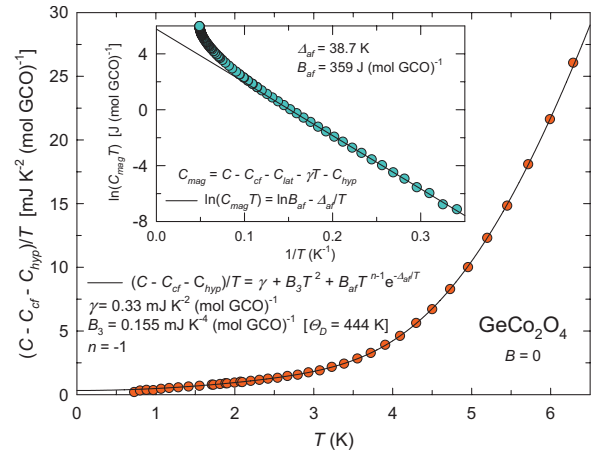


FIG. 20. (Color) Plot of the specific-heat data for $B=0$ as $(C-C_{\text{cf}}-C_{\text{hyp}})/T$ vs T for $T < 6.5$ K; see the text for the procedure used to determine the C_{hyp} term for ^{59}Co —Sec. IV B. The expression used for the fitting is $(C-C_{\text{hyp}}-C_{\text{cf}}) = \gamma T + B_3 T^3 + B_{\text{af}} T^n e^{-\Delta_{\text{af}}/T}$ which is described in Sec. IV B. Fit parameters are tabulated in the figure. In the inset, the anisotropic gapped spin-wave contribution to the low-temperature specific heat, $C_{\text{mag}} = C - C_{\text{cf}} - C_{\text{lat}} - \gamma T - C_{\text{hyp}}$, is plotted as $\ln(C_{\text{mag}}T)$ vs $1/T$. The straight line through the points is calculated from the fit parameters and is valid up to ~ 7 K ($\sim 1/3T_N$). There is scatter in C_{mag} below ~ 2.5 K, which increases as T decreases since C_{mag} below ~ 2.5 K is nearly zero and the small residuals include all of the experimental measurement errors.

sociated with these energy levels, which is shown as the blue curve in Fig. 19, and whose contribution to C is negligible below ~ 5 K. Since the degeneracies of the Kramers doublets are removed in a magnetic field—by an unknown amount— C_{cf} will be field dependent. However, the expected splitting of the doublets by the fields used for the present measurements should produce only small separations with respect to the energy of the crystal-field levels above the ground state. Consequently, $C_{cf}(B)$ should be essentially the same as $C_{cf}(0)$.

The specific heats for $B=0$, measured at BYU, are shown as red squares in Fig. 19, and the green triangles are the specific heats after subtracting C_{cf} . The expression used to fit $(C-C_{cf})$ in the range $23 \text{ K} \leq T \leq 75 \text{ K}$ is the same as that given in Fig. 14 plus a γT term representing a contribution from oxygen defects—see below for its origin and a discussion of how it was determined. When possible, it is generally better to determine B_3 from a low-temperature fit and then use that value held fixed in the expression for the fit at high temperatures to determine C_{lat} . It was determined that GCO has no $B_{af}T^3$ spin-wave contribution at low temperatures and $B_3=0.155 \text{ mJ K}^{-4} (\text{mol GCO})^{-1}$ was determined from the low-temperature fit as was $\gamma = 0.33 \text{ mJ K}^{-2} (\text{mol GCO})^{-1}$ —see below and Fig. 19. There is a small anomaly in C/T centered at ~ 31 K that is associated with a GeCoO_3 impurity phase, which has an antiferromagnetic transition at that temperature with an unknown specific heat.⁷ X-ray- and neutron-diffraction measurements for the GCO sample identified this impurity phase and provided an estimate of the amount present: ~ 3 wt %.⁴ Data in the region of that anomaly, from ~ 28 to ~ 33 K, are not included in the fit, which has an rms of 0.8%. The black curve through the green triangles represents the fit and the pink curve represents C_{lat} . The Debye theta Θ_D is larger for GCO (444 K) than for GNO (386 K), which makes the GCO lattice the stiffer of the two.

A plot of $(C-C_{cf})/T$ vs T^2 for the $B=0$ data measured at BYU—not shown—has an upturn at the lower temperatures and a linear region to ~ 3 K that extrapolates to a positive intercept at $T=0$. A preliminary fit of the specific-heat data in the region for $T \leq 3$ K to $(C-C_{cf})=D/T^2 + \gamma T + B_3 T^3$ enables a determination of the hyperfine contribution to the specific heat from ^{59}Co : $C_{hyp}=1.41 \times 10^{-3} \text{ T}^{-2} \text{ J K}^{-1} (\text{mol GCO})^{-1}$. With $D=1.41 \times 10^{-3} \text{ J K} (\text{mol GCO})^{-1}$ and using Eq. (6), the hyperfine field at the Co^{2+} nuclei is $B_n=129$ T.

Figure 20 is a plot of $(C-C_{cf}-C_{hyp})/T$ vs T for $T < 6.5$ K. Through trial and error it was found that the specific heat at low temperatures cannot be represented by a $B_{af}T^3$ spin-wave contribution. The low-temperature fitting expression is $(C-C_{hyp}-C_{cf})=\gamma T + B_3 T^3 + B_{af} T^n e^{-\Delta_{af}/T}$. The gap in the spin-wave spectrum probably has its origin in the splitting of the ground-state $J=1/2$ Kramers doublet induced by the exchange interaction. Since GCO is an insulator, the γT term is not associated with conduction electrons but most likely has its origin in oxygen defects in the crystal with the linear term related to vibrations of trapped particles in those voids.^{23,24} Linear terms of this magnitude are commonly observed in the specific heats of many insulating substances containing oxygen—see, e.g., Ref. 25. The downturn in C/T at the lower temperatures is probably not related to a prop-

erty of the compound but has its origin in small errors in the calorimeter addenda and/or temperature-scale calibrations. A least-squares fit is made to the specific-heat data in the range $1.4 \text{ K} \leq T \leq 6.5 \text{ K}$. Data below 1.4 K are excluded from the fit since the values are very small and have greater errors. Fits with n held fixed at positive and negative integers has a minimum rms at $n=-1$; when included in a fit $n=-0.99$. The fit, with n fixed at -1 , has an rms of 1.0%; the parameters are given in Fig. 20. The first term of the harmonic-lattice expression, $B_3=0.155 \text{ mJ K}^{-4} (\text{mol GCO})^{-1}$, was fixed in the fit above T_N shown in Fig. 19 as was $\gamma = 0.33 \text{ mJ K}^{-1} (\text{mol GCO})^{-1}$.

In the inset of Fig. 20 the anisotropic spin-wave contribution to the low-temperature specific heat, $C_{mag}=C-C_{cf}-C_{lat}-\gamma T-C_{hyp}$, is shown as a plot of $\ln(C_{mag}T)$ vs $1/T$. The straight line through the points is calculated from the fit parameters and is valid up to ~ 7 K or $\sim 1/3T_N$. The gap in the antiferromagnetic spin-wave spectrum, $\Delta_{af}=38.7$ K, is also observed in neutron-scattering spectroscopy—see Fig. 21.⁴ Since the spin-wave gap shown in Fig. 21 has a temperature dependence and goes to zero as $T \rightarrow T_N$, the 38.7 K gap derived from the fit to the low-temperature specific-heat data is necessarily an average.

Figure 22 is a plot of $C_{mag}(B)$ vs T for the LANL data in the temperature region below 7.5 K for fields up to 9 T. Because the lowest temperatures of the measurements are ~ 1.9 K, no $C_{hyp}(B)$ from ^{59}Co is detected. As B increases, $C_{mag}(B)$ vs T increases monotonically. No theoretical fits are made to the data because it is not known how a magnetic field will modify the gapped spin waves. In addition, there will be magnetic-domain alignment in applied magnetic fields, which will further complicate the interpretation.

The magnetic entropy S_{mag} for GCO is obtained by a numerical evaluation of $\int (C_{mag}/T)dT$ in the range $0 \text{ K} \leq T \leq 75 \text{ K}$ plus the contribution from 75 K to ∞ , which is assumed to be $(A_2/3T^3 + A_3/4T^3)$ evaluated at 75 K—see Fig. 19. Figure 23 plots C_{mag}/T vs T and S_{mag} vs T for the BYU data for $B=0$; the inset shows S_{mag} vs T , on an expanded scale, in the vicinity of T_N . The entropy recovered from the magnetic specific-heat analysis is $S_{mag}=6.72 \text{ J K}^{-1} (\text{mol GCO})^{-1}$. Of this $\sim 3.7 \text{ J K}^{-1} (\text{mol GCO})^{-1}$ is recovered below T_N and $\sim 3.0 \text{ J K}^{-1} (\text{mol GCO})^{-1}$ above. At the first-order transition the entropy change is $0.439 \text{ J K}^{-1} (\text{mol GCO})^{-1}$ —see the inset of Fig. 23. The related enthalpy (latent heat) at the transition is $\Delta H=9.06 \text{ J} (\text{mol GCO})^{-1}$.

If the ground state of Co^{2+} in GCO has $J=1/2$, the entropy associated with the ordering is $2R \ln(2J+1) = 11.53 \text{ J K}^{-1} (\text{mol GCO})^{-1}$. Only 58.3% of this is recovered, which is nearly the same as that for GNO, for which 56.5% was recovered. As was discussed for GNO in Sec. IV B, it is shown that there is no hidden ordering or magnetic disorder in the ground state, which could account for the missing entropy. The analysis shown in Fig. 9 conclusively demonstrates that the specific heats and entropies well above T_N for all B are the same to within the experimental accuracy. As for GNO, the missing entropy could be explained by substantial magnetic correlations above T_N —see Sec. VI C.

Similar to GNO, the entropy-conserving construction shown in the inset of Fig. 23 has a $T_N(0)$ that is slightly

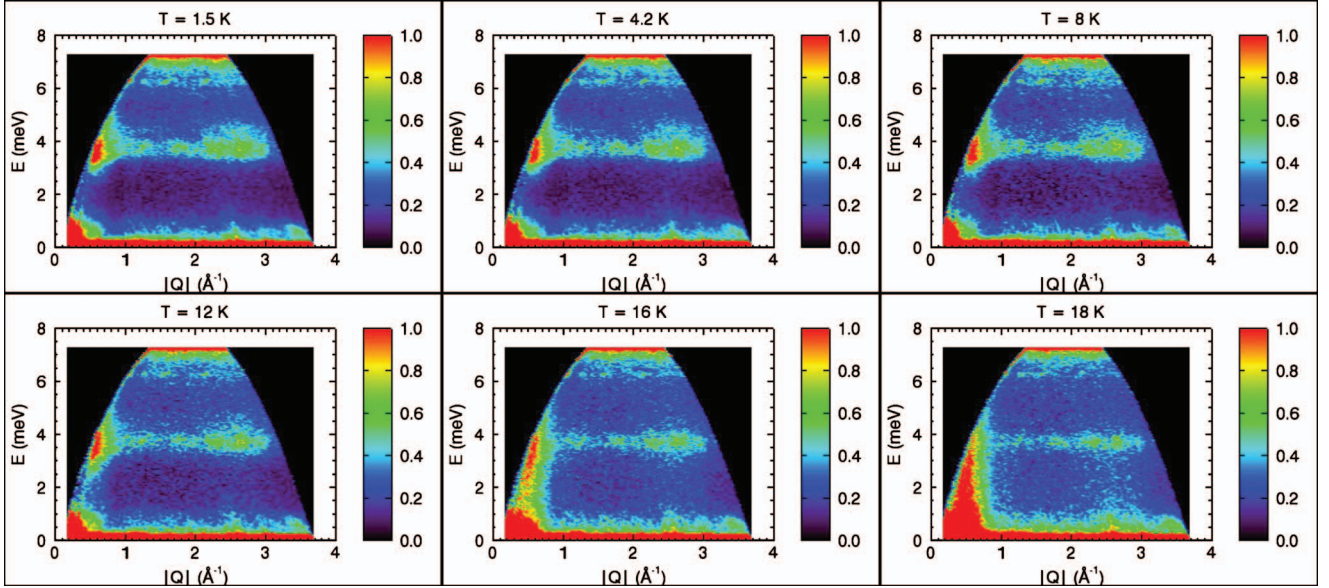


FIG. 21. (Color) Inelastic-neutron-scattering spectrum for polycrystalline GCO measured at temperatures in the range $1.5 \text{ K} \leq T \leq 18 \text{ K}$ using the disk chopper spectrometer (Ref. 11) at the NIST Center for Neutron Research. The incident-neutron wavelength was 3.2 \AA . At the antiferromagnetic wave vector $Q=0.65 \text{ \AA}^{-1}$ there is an energy gap at 1.5 K in the magnetic excitations of $E \sim 3 \text{ meV}$ ($\sim 35 \text{ K}$). As the temperature is increased the gap decreases and vanishes as $T \rightarrow T_N$.

different from the $T_N(0)$ that is defined by the maximum in $C(0)/T$. The difference is only $\sim 0.03 \text{ K}$ and, although T_N from the entropy-conserving construction is more nearly correct, $T_N(B)$ will continue to be defined as T at the maximum of $C(B)/T$.

V. SPECIFIC-HEAT AND MAGNETIZATION MEASUREMENTS BY OTHERS

Hubsch and Gavaille²⁶ measured the magnetic susceptibility for GCO and interpreted the irreversibility near T_N for field-cooled (FC) and zero-field-cooled (ZFC) measurements as demonstrating that the antiferromagnetic transition is first

order. Their paper contains references to earlier measurements on GCO. Zero-field specific-heat and field-swept directional-magnetization measurements were made for a GNO single crystal, which shows a field-induced anisotropy below T_{N1} and a possible third transition below T_{N2} —a small anomaly is observed as in the present measurements.²⁷ Magnetization measurements were made by Diaz *et al.*^{16,28,29} on polycrystalline GNO and GCO to fields of 55 T. They found that both compounds have two magnetic moment reorienta-

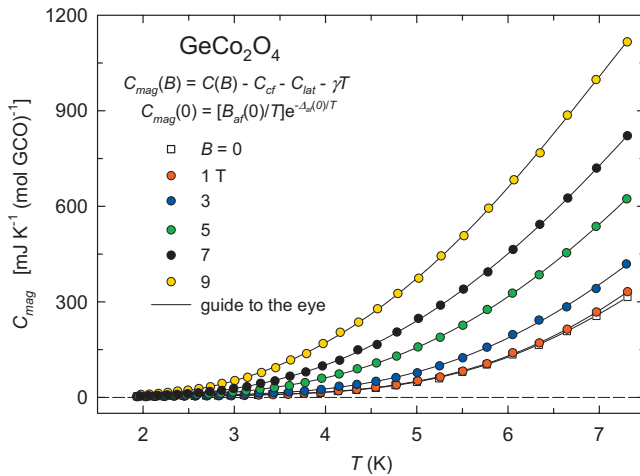


FIG. 22. (Color) $C_{\text{mag}}(B)$ vs T showing the evolution of the gapped spin-wave contribution to the specific heat for $0 \text{ T} \leq B \leq 9 \text{ T}$. The curves through the data are guides to the eye except for $C_{\text{mag}}(0)$.

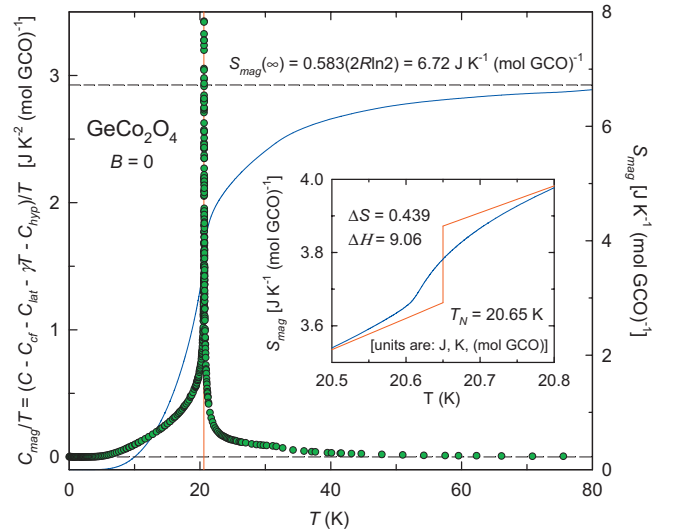


FIG. 23. (Color) C_{mag}/T vs T and S_{mag} vs T for the $B=0$ specific-heat data. The inset shows S_{mag} vs T , on an expanded scale, in the vicinity of T_N , in addition to an entropy-conserving construction for evaluation of the entropy and latent heat associated with the transition. This figure is similar to Fig. 18 for GNO. Note: The units of S are $\text{J K}^{-1} (\text{mol GCO})^{-1}$ and for H are $\text{J} (\text{mol GCO})^{-1}$.

tions (spin flops) and that 55 T is insufficient to attain magnetic saturation. By failing to take into account crystal-electric-field levels, they incorrectly interpreted their GCO susceptibility measurements¹⁶ as showing ferromagnetic interactions—see Sec. II B2 and Figs. 11 and 12. Hoshi *et al.*¹⁷ measured the magnetization and susceptibility of a single crystal of GCO as a function of temperature in fields up to 12 T applied along the (111), (110), and (100) directions. They interpreted their susceptibility data using the Curie-Weiss law. However they also neglected to take into account contributions from the crystal-electric-field levels and consequently derived an incorrect ferromagnetic $T_W = 40$ K. Lancaster *et al.*³⁰ measured specific heats in the vicinity of the transition temperatures for polycrystalline GNO in $B=0, 7$, and 14 T, with results that are in reasonable agreement with those reported here.

$\text{Gd}_2\text{Ti}_2\text{O}_7$ is a pyrochlore, with spins on corner-shared tetrahedra, that orders antiferromagnetically with two transitions in the specific heat^{31,32} at ~ 0.7 and ~ 1 K, which is qualitatively similar to GNO. In zero magnetic field the recovered entropy is determined^{31,32} by integration of C/T vs T and equals the expected $2R \ln 8$ at ~ 10 K, which shows that the ground state at $T=0$ has no magnetic disorder.³² One set of data³¹ extends to ~ 0.1 K and has an anomaly in C/T vs T beginning at ~ 0.2 K that is similar to the 5-K anomaly observed for GNO. No analysis of the low-temperature data is made. The other set of data³² extends only up to ~ 0.4 K and the authors pointed to a $C \propto T^2$ dependence from ~ 0.4 to ~ 0.6 K. This T^2 dependence over a limited temperature range cannot be interpreted as a property of the ground state since power-law approximations to antiferromagnetic order apply only at temperatures below $\sim 1/2$ to $\sim 1/3 T_N$ —see below for the ground state for $\text{Gd}_2\text{Sn}_2\text{O}_7$. It is suggested^{32,33} that the two anomalies in the specific heat correspond to a partial ordering of the spins on a kagome lattice at ~ 1 K, which is followed by a transition at ~ 0.7 K to a state that becomes fully ordered at $T=0$. The conjecture was later confirmed by neutron-diffraction measurements.³⁴ This kind of ordering is similar to the one proposed for GNO, although in $\text{Gd}_2\text{Ti}_2\text{O}_7$ a 4- k magnetic structure has been demonstrated while in GNO it appears that a 1- k structure is correct.¹³

Another antiferromagnetic pyrochlore, $\text{Gd}_2\text{Sn}_2\text{O}_7$, has a single specific-heat anomaly at ~ 1 K.³⁵ At low temperatures the specific heat is fit by a gapped spin-wave expression of the form $C = BT^{-2}e^{-\Delta/T}$ valid up to ~ 0.3 K ($\sim 1/3 T_N$). It also exhibits a $C \propto T^2$ behavior from ~ 0.4 to ~ 0.8 K. The entropy was not evaluated.

VI. SUMMARY AND CONCLUSIONS

Specific-heat and magnetic-susceptibility measurements were made on polycrystalline samples of the spinels GNO and GCO in the range $0.5 \text{ K} \leq T \leq 400 \text{ K}$ in magnetic fields up to 14 T. They order out of different ground states: $S=1$ and $J=1/2$, respectively. Both compounds have first-order antiferromagnetic transitions with a closely spaced double transition for GNO that is probably associated with separate ordering on the kagome and triangular planes.^{5,13} Below T_{N2} there is a small anomaly centered at ~ 11 K for $B=0$ and 1

T, which might represent a rearrangement of the magnetic moments. There is a fourth anomaly centered at ~ 5 K that is linked to gapped antiferromagnetic spin waves, which is observed in all fields up to 14 T. Concurrently, there are ungapped antiferromagnetic spin waves. GCO has only gapped antiferromagnetic spin waves with the gap collapsing as $T \rightarrow T_N$. In magnetic fields the specific-heat anomalies for both compounds move to lower temperatures as expected for antiferromagnetic ordering but at a surprisingly much slower rate for GNO even though the $T_N(0)$ are $\sim 1/2 T_N(0)$ for GCO. The results of the measurements, combined with the data analysis, show clearly that the different ground states for the two compounds have a profound effect on their antiferromagnetic ordering.

A. GeNi_2O_4

The crystal-electric-field states for GNO are sufficiently removed from the $S=1$ manifold that they make no contribution to the specific heat or susceptibility for $T < 400$ K. Below T_{N2} the antiferromagnetic ordering has both gapped and ungapped spin waves present. The spin waves with a 10.9-K gap are associated with the 5-K anomaly—see Figs. 15 and 16. Splitting of the $S=1$ multiplet amplified by the antiferromagnetic-exchange interaction is probably the source of the 10.9-K gap, which is also observed in neutron-scattering spectroscopy—see Fig. 15.⁵ The simultaneous occurrence of both gapped and ungapped spin waves in an antiferromagnetically ordered substance is very unusual and perhaps lends support to the proposal¹³ that the kagome and triangular planes order separately.

A numerical evaluation of $\int (C_{\text{mag}}/T) dT$ determines S_{mag} , and only 56.5% of the expected $S_{\text{mag}} = 2R \ln(2S+1) = 18.27 \text{ J K}^{-1} (\text{mol GNO})^{-1}$ is recovered, i.e., $10.33 \text{ J K}^{-1} (\text{mol GNO})^{-1}$. The missing entropy is $7.94 \text{ J K}^{-1} (\text{mol GNO})^{-1}$. Although antiferromagnetic ordering in spinels can have frustration, the specific-heat measurements in magnetic fields show that the entropies and specific heats well above T_{N1} are the same for all B . If there is hidden ordering for $T < 0.5$ K, or magnetic disorder in the ground state, then $S_{\text{mag}}(9) > S_{\text{mag}}(0)$ and $C(B) > C(0)$ well above T_{N1} , which is not observed. The missing entropy could be a result of substantial magnetic correlations well above the Néel temperatures—see Sec. VI C.

A Curie-Weiss law fit of χ^{-1} vs T for $B=5$ T, in the range $150 \text{ K} \leq T \leq 400 \text{ K}$, has a negative Weiss constant, $T_W = -8.7$ K, indicating antiferromagnetic interactions and in satisfactory agreement with T_{N1} from the specific-heat measurements. The associated $p = g[S(S+1)]^{1/2} = 3.32$ and $g = 2.35$ are in the range found for Ni^{2+} ions in a trigonal crystal-field.² The ratio $T_W/T_{N1}(0) = 0.7$ indicates that GNO is not frustrated.¹⁴

B. GeCo_2O_4

A Co^{2+} free ion has a ${}^4\text{F}_{9/2}$ ground state that is split in GCO into six Kramers doublets at 0, 180, 360, 440, 1760, and 1930 K.⁴ The crystal-electric-field levels above the ground state will contribute to the specific heat and, unlike GNO, must be taken into account in the analysis to deter-

mine C_{mag} . The onset of cooperative long-range antiferromagnetic order is at $T_N=20.617$ K. In $B=0$ the specific heat has a small γT term, with $\gamma=0.33$ mJ K⁻² (mol GCO)⁻¹, that is related to oxygen defects.^{23–25} The ⁵⁹Co nuclei have a hyperfine specific heat for $B=0$ produced by a field at the nuclei, $B_n=129$ T. At temperatures below T_N the specific heat for $B=0$ is fitted by using $B_{\text{af}}T^{-1}e^{-\Delta_{\text{af}}/T}$, which confirms spin-wave ordering with a gap of 38.7 K induced by the antiferromagnetic-exchange-interaction splitting of the $J=1/2$ ground state. This energy gap is also observed⁴ in neutron-scattering spectroscopy—see Fig. 21.

The field-dependent tetragonal-to-cubic lattice transition is uncovered as increasing magnetic fields shift the antiferromagnetic anomalies to lower temperatures. A small anomaly is coupled to this transition with an associated enthalpy/latent heat of ~ 0.3 J (mol GCO)⁻¹ and an entropy of ~ 0.015 J K⁻¹ (mol GCO)⁻¹.

The $J=1/2$ ground state has an expected $S_{\text{mag}}=2R \ln(2J+1)=11.53$ J K⁻¹(mol GCO)⁻¹. However, there is only 6.72 J K⁻¹(mol GCO)⁻¹—58.3% of the projected amount—recovered from an analysis of C_{mag} , which is nearly identical to that for GNO. The missing entropy is 4.81 J K⁻¹ (mol GCO)⁻¹. As for GNO, magnetic correlations, and not hidden ordering or magnetic disorder in the ground state, could explain the missing entropy—see Sec. VI C.

The Curie-Weiss law cannot be used for GCO because of contributions from the excited crystal-electric-field levels that cause curvature to $\chi^{-1}(B)$ vs T . There are several invalid applications^{16,17} of the Curie-Weiss law to GCO that derive a positive Weiss constant that incorrectly indicates ferromagnetic interactions.

C. Magnetic correlations in the paramagnetic phase

One of the interesting aspects of the magnetic order in GNO and GCO are the significant missing magnetic entropies: 43.5% and 41.7%, respectively. We believe that our in-field specific-heat measurements eliminate the possibility that residual entropy is present at low temperatures in these materials; certainly not the amounts that are missing. We, therefore, conclude that the missing entropy must arise from substantial magnetic correlations at relatively high temperatures that we are not accounting for in our lower-temperature analysis of the specific-heat data.

The specific-heat analysis shows that after subtracting our derived values for the lattice contributions up to 75 K, the magnetic contributions above T_N essentially vanish by the time we reach that temperature—see Figs. 18 and 23. However, because of the increasing lattice contributions and diminishing magnetic contributions (see Figs. 13 and 19) as the temperature increases, it is conceivable—but improbable—that the methods of analysis used overestimate the lattice contributions and underestimate the magnetic contributions to the specific heat.

There are other materials where such an entropy shortfall has been reported. For example, in SrCr_{9x}Ga_{12-9x}O₁₉, a material with a crystal structure related to the spinels (kagome bilayers separated by triangular layers), only 50% of the ex-

pected entropy is recovered up to 100 K.³⁶ Long-range magnetic order does not appear in this system down to temperatures as low as 0.05 K, and this was described as resulting from the formation of a spin-liquid state at low temperature. At higher temperatures spin singlets were suggested to be present and responsible for the missing entropy. In this material the Weiss constant is large, $T_W=-500$ K, which makes the existence of spin singlets at temperatures above 100 K reasonable. Of course, in GNO the Weiss constant is much smaller and attributing the entropy shortfall in those materials to some form of magnetic correlations at temperatures above 75 K is not as compelling. However, initial measurements on GCO single crystal have directly revealed the presence of substantial magnetic correlations, as demonstrated by the presence of clear structure in the paramagnetic neutron scattering at temperatures at least as high as 100 K.³⁷ Thus, there is indeed some reason to believe that more entropy could appear at temperatures above 75 K in that material.

It is also worth commenting on the fact that magnetic correlations in GNO and GCO exist up to temperatures considerably above the Néel transitions. In GNO, where the Weiss temperature is $T_W=-8.7$ K, significant magnetic correlations exist up to at least $T=125$ K as judged by the magnetic susceptibility (Fig. 10) and the specific heat (Fig. 18). Thus, in some ways, these materials are similar to low-dimensional antiferromagnets, where the 3-D ordering temperatures are determined by weak interchain or interplane magnetic interactions, while the correlations at higher temperatures are a result of the stronger intrachain or intraplane interactions. In addition, in lower-dimensional antiferromagnets, the amount of entropy associated with 3-D order is generally quite small compared with the value expected for the spin magnitudes involved since much of the entropy is destroyed by correlations above the Néel transitions or by fluctuations below the transitions. GNO does not fall into the category of highly frustrated antiferromagnets based upon the ratio of the Weiss temperature to the Néel transition temperature.¹⁴ In fact, for GNO, the ratio is close to unity, suggesting no frustration effects at all.

In conclusion, the observation that both GNO and GCO do not exhibit the amounts of entropy expected for their ground states remains a question for future research. The presence of an energy gap in the specific-heat and inelastic-neutron-scattering data is also particularly interesting for GNO since it coexists with ungapped spin-wave excitations. These two forms of magnetic excitations might be associated with the kagome and triangular planes, which would suggest that these planes are weakly coupled, perhaps due to frustration introduced by the specific form of the magnetic order along the [111] direction.¹³ Finally, in GNO and GCO, one expects rather weak intralayer nearest-neighbor ferromagnetic interactions in the (111) planes but stronger interactions between the planes mediated by further neighbor exchange.¹³ A complete understanding of the magnetic order and excitations will require quantitative determinations of the signs and magnitudes of the different magnetic-exchange interactions in each material by inelastic-neutron-scattering measurements using high-quality, single-crystal samples. The

specific-heat measurements reported here will provide a quantitative test of any models proposed for these materials.

D. Comparison to triangular or kagome magnets: Low-temperature behavior and magnetic entropy

The presence of both triangular and kagome planes in GNO and GCO suggests that comparison of the specific-heat results described in this paper to both theoretical predictions for triangular and kagome antiferromagnets (TAFM and KAFM, respectively), as well as experimental results for other materials that consist of triangular and/or kagome planes, might be useful. However, the low-temperature magnetic structure of GNO and GCO consists of ferromagnetic (111) kagome and triangular planes with antiferromagnetic interplanar order. This implies that the excitations we observe in GNO or GCO are likely to have little relevance to those of 2-D kagome or triangular antiferromagnets³⁸ but must instead be associated with the three-dimensional antiferromagnetic state of each material. If indeed the kagome and triangular layers order independently in GNO¹³ and are weakly coupled together due to the presence of magnetic frustration, then the relevant excitations are those of 3-D kagome and triangular antiferromagnets consisting of antiferromagnetically coupled ferromagnetic planes. On this model the coexistence of isotropic (ungapped) 3-D spin waves and anisotropic (gapped) 3-D spin waves can be attributed to the kagome or triangular layers. This coexistence of two nearly independent spin systems in GNO, each composed of Ni²⁺ ions located on identical crystallographic sites, is interesting and perhaps unique. It is unlikely that the gapped excitations in GNO reflect anything other than gapped spin waves since the neutron-scattering data show nicely dispersing excitations above the gap at 0.65 Å⁻¹—see Ref. 5 and Fig. 15. Of course it would be of interest to know which Ni²⁺ site supports which type of excitation and then to develop some theoretical understanding for the origin of their different be-

haviors. The single-ion anisotropies on the two sites should be identical (other than the interchange of the unique axis for the trigonal field), so the appearance of a gap in one excitation spectrum but not the other is strange. There is some evidence in the inelastic-neutron-scattering spectrum of GNO at momentum transfers greater than 2.0 Å⁻¹ for additional spin waves that may not be gapped. However that observation suffers from a low signal-to-noise ratio and should be repeated using longer integration times or, better yet, single crystals.

The GCO results are easier to understand than those for GNO. The empirical fit of the specific-heat data for GCO to a fully gapped spin wave is consistent with a 3-D Ising antiferromagnet whose Kramers doublet ground state is split by the exchange interaction. This gap is also observed in the inelastic-neutron-scattering spectrum—see Ref. 4 and Fig. 21. There is a single magnetic transition at which both the kagome and triangular layers order in this material.

ACKNOWLEDGMENTS

The authors acknowledge E. M. McCarron, R. J. Smalley, T. Borecki, and J. Hormadaly for help with sample preparation. They thank J. R. D. Copley of the NIST Center for Neutron Research for his continuing interest and helpful discussions on the neutron-scattering experiments. Research at Los Alamos National Laboratory was supported by the U.S. Department of Energy under Grant No. DEFG-03-86ER-45230 and the U.S. National Science Foundation (NSF) under Grant No. DMR-00-72125, and was performed under the auspices of the NSF, the State of Florida, the National Nuclear Security Administration, and the U.S. Department of Energy. The Office of Research and Creative Activities at BYU provided funding for support of the BYU research. This work utilized facilities, supported in part, by the National Science Foundation under Agreement No. DMR-0454672.

¹E. F. Bertaut, V. V. Qiu, R. Pauthenet, and A. Murasik, *J. Phys. (France)* **25**, 516 (1964).

²W. Low, *Paramagnetic Resonance in Solids*, Solid State Physics Suppl. 2 (Academic, New York, 1960), pp. 92–105; A. Abragam and B. Bleaney, *Electron Paramagnetic Resonance of Transition Ions* (Oxford, New York, 1970), p. 449.

³W. Low, *Paramagnetic Resonance in Solids*, Solid State Physics Suppl. 2 (Academic, New York, 1960), pp. 40–42; A. Abragam and B. Bleaney, *Electron Paramagnetic Resonance of Transition Ions* (Oxford, New York, 1970), p. 446.

⁴M. K. Crawford, R. L. Harlow, P. L. Lee, Y. Zhang, J. Hormadaly, R. Flippen, Q. Huang, J. W. Lynn, Y. Qiu, J. R. D. Copley, R. Stevens, B. F. Woodfield, J. Boerio-Goates, and R. A. Fisher (unpublished).

⁵M. K. Crawford, R. L. Harlow, P. L. Lee, Y. Zhang, J. Hormadaly, R. Flippen, Q. Huang, J. W. Lynn, R. Stevens, B. F. Woodfield, J. Boerio-Goates, and R. A. Fisher, *Phys. Rev. B* **68**, 220408(R) (2003).

⁶P. A. Goddard, A. V. Silhanek, J. C. Lashley, M. Jaime, J. Singleton, R. A. Fisher, and M. K. Crawford (unpublished).

⁷R. Stevens, B. F. Woodfield, J. Boerio-Goates, and M. K. Crawford, *J. Chem. Thermodyn.* **36**, 359 (2004).

⁸R. Stevens and J. Boerio-Goates, *J. Chem. Thermodyn.* **36**, 857 (2004).

⁹B. F. Woodfield, Ph.D. thesis, University of California, 1995.

¹⁰J. C. Lashley, M. F. Hundley, A. Migliori, J. L. Sarrao, P. G. Pagliuso, T. W. Darling, M. Jaime, J. C. Cooley, W. L. Hults, L. Morales, D. J. Thoma, J. L. Smith, J. Boerio-Goates, B. F. Woodfield, G. R. Stewart, R. A. Fisher, and N. E. Phillips, *Cryogenics* **43**, 369 (2003).

¹¹J. R. D. Copley and J. C. Cook, *Chem. Phys.* **292**, 477 (2003).

¹²M. F. Collins and O. A. Petrenko, *Can. J. Phys.* **75**, 605 (1997); W. B. Yelon and D. E. Cox, *Phys. Rev. B* **7**, 2024 (1973); H. Kadowaki, K. Ubukoshi, and K. Hirakawa, *J. Phys. Soc. Jpn.* **56**, 751 (1987).

¹³M. Matsuda, J.-H. Chung, S. Park, T. J. Sato, K. Matsuno, H.

- Aruga Katori, H. Takagi, K. Kakurai, K. Kamazawa, Y. Tsunoda, I. Kagomiya, C. L. Henley, and S.-H. Lee, arXiv:0708.3162 (unpublished).
- ¹⁴A. P. Ramirez, *Annu. Rev. Mater. Sci.* **24**, 453 (1994).
- ¹⁵C. J. Ballhausen, *Introduction to Ligand Field Theory* (McGraw-Hill, New York, 1962), p. 128.
- ¹⁶S. Diaz, S. de Brion, M. Holzapfel, G. Chouteau, and P. Strobel, *Physica B (Amsterdam)* **346-347**, 146 (2004).
- ¹⁷T. Hoshi, H. Aruga Katori, M. Kosaka, and H. Takagi, *J. Magn. Magn. Mater.* **310**, e448 (2007).
- ¹⁸A. Abragam and M. H. L. Pryce, *Proc. R. Soc. London, Ser. A* **206**, 173 (1951); J. B. Goodenough, *Phys. Rev.* **171**, 466 (1968).
- ¹⁹E. S. R. Gopal, *Specific Heats at Low Temperatures* (Plenum, New York, 1966), Chap. 2; M. Blackmann, *Rep. Prog. Phys.* **26**, 1 (1941).
- ²⁰J. H. van Vleck, *Electric and Magnetic Susceptibilities* (Oxford University Press, New York, 1959); R. L. Carlin and A. J. van Duyneveldt, *Magnetic Properties of Transition Metal Compounds* (Springer-Verlag, New York, 1977); N. E. Phillips and R. A. Fisher, in *Encyclopedia of Condensed Matter Physics*, edited by G. F. Bassani, G. L. Liedel, and P. Wyder (Elsevier, United Kingdom, 2005).
- ²¹J. van Kranendonk and J. H. van Vleck, *Rev. Mod. Phys.* **30**, 1 (1958); E. S. R. Gopal, *Specific Heats at Low Temperatures* (Plenum, New York, 1966), p. 91.
- ²²C. Kittel, *Introduction to Solid State Physics*, 6th ed. (Wiley, New York, 1986), p. 426.
- ²³H. R. Rosenstock, *J. Phys. Chem. Solids* **23**, 659 (1962); H. R. Rosenstock, *Am. J. Phys.* **30**, 38 (1962); H. R. Rosenstock, *J. Non-Cryst. Solids* **7**, 123 (1972).
- ²⁴R. A. Fisher, *J. Non-Cryst. Solids* **41**, 251 (1980).
- ²⁵J. M. D. Coey, S. von Molnar, and A. Torressen, *J. Less-Common Met.* **151**, 191 (1989).
- ²⁶J. Hubsch and G. Gavoille, *J. Magn. Magn. Mater.* **66**, 17 (1987).
- ²⁷S. Hara, Y. Yoshida, S.-I. Ikeda, N. Shirakawa, M. K. Crawford, K. Takase, Y. Takano, and K. Sekiwaza, *J. Phys. Soc. Jpn.* **73**, 2959 (2004).
- ²⁸S. Diaz, S. de Brion, G. Chouteau, P. Strobel, B. Canals, J. R. Carvajal, H. Rakoto, and J. M. Broto, *J. Appl. Phys.* **97**, 10A512 (2005).
- ²⁹S. Diaz, S. de Brion, G. Chouteau, B. Canals, V. Simonet, and P. Strobel, *Phys. Rev. B* **74**, 092404 (2006).
- ³⁰T. Lancaster, S. J. Blundell, D. Prabhakaran, P. J. Baker, W. Hayes, and F. L. Pratt, *Phys. Rev. B* **73**, 184436 (2006).
- ³¹A. P. Ramirez, B. S. Shastry, A. Hayashi, J. J. Krajewski, D. A. Huse, and R. J. Cava, *Phys. Rev. Lett.* **89**, 067202 (2002).
- ³²O. A. Petrenko, M. R. Lees, G. Balakrishnan, and D. McK Paul, *Phys. Rev. B* **70**, 012402 (2004).
- ³³J. D. M. Champion, A. S. Wills, T. Fennell, S. T. Bramwell, J. S. Gardner, and M. A. Green, *Phys. Rev. B* **64**, 140407(R) (2001).
- ³⁴J. R. Stewart, G. Ehlers, A. S. Wills, S. T. Bramwell, and J. S. Gardner, *J. Phys.: Condens. Matter* **16**, L321 (2004).
- ³⁵J. A. Quilliam, K. A. Ross, A. G. Del Maestro, M. J. P. Gingras, L. R. Corruccini, and J. B. Kycia, *Phys. Rev. Lett.* **99**, 097201 (2007).
- ³⁶A. P. Ramirez, B. Hessen, and M. Winklemann, *Phys. Rev. Lett.* **84**, 2957 (2000).
- ³⁷M. K. Crawford, P. Manuel, D. T. Adroja, S. I. Ikeda, S. Hara, and J. W. Lynn (unpublished).
- ³⁸G. Misguich and C. Lhuillier, in *Frustrated Spin Systems*, edited by H. T. Diep (World Scientific, New Jersey, 2004), Chap. 5.